GREEN SYNTHESIS OF AN AMIDE-BASED CHEMOSENSOR AND ITS APPLICATION FOR DETECTION OF TOXIC METAL IONS

D. S. Bhagat,[a]* R. P. Pawar,[b]* A. B. Tekale,[c] S. G. Pande,[a] R. R. Rangari,[a] I. V. Suryawanshi,[a] P. B. Chavan[a], S. N. Tapase[a] and A. A. Sahu[d]

Keywords:chemosensor,forensic application,ultra-sonication,coordination complex

Ultrasound-assisted synthesis of a chemosensor from benzoyl chloride and diethylenetriamine in acetonitrile was carried out and the product structure was confirmed by UV-VIS and FT-IR spectroscopy. The synthesized chemosensor interacts with metal ions and produces a notable change in colorimetric measurements. It is observed that as the concentration of metallic ions increases, absorbance also increases, thus the chemosensor can be used for quantitative estimation of metal-ion content.

* Corresponding Authors
E-Mail: rppawar@yahoo.com
[a] Department of Forensic Chemistry and Toxicology, Government Institute of Forensic Science, Aurangabad-431005 (M.S.)
[b] Department of Chemistry Deogiri College, Station Road, Aurangabad 431 005, Maharashtra, India
[c] Department of Chemistry, Shri Shivaji College, Parbhani – 431 401 (MS) India.
[d] Department of Forensic Chemistry and Toxicology, Government Institute of Forensic Science, Aurangabad-431005 (M.S.)

Introduction

In recent decade increase in industrialization resulted in high pollution of metal ions in the environment which interact with living systems and cause hazardous effects on human health and the environment resulting in toxic cation and poisoning.

Chemosensor is a sensory receptor that shows a detectable change in color and photophysical properties. The ultimate aim of the scientific community is the synthesis of sensitive chemosensor which can be used for the detection of heavy metal ions.[1] The Hg^{2+} is a common, environmentally toxic and hazardous pollutant among the heavy metal ions. Trace amounts of Hg^{2+} in the body can lead neurotoxicity and the mercury ions easily pass through the biological tissues to cause digestive, kidney and especially neurological diseases.[2] The Cu^{2+} ion is an important transitional metal ion which plays a major role in environmental, biological, forensic and chemical fields.[3] Cu^{2+} ion is the third most abundant essential metal ion in the human body transition element after Fe^{3+} and Zn^{2+}.[4] Zinc is the second most abundant transition metal in the human body next to iron and acts as a catalytic co-factor in various metallic-enzymes. Zn^{2+} ions play a vital role in numerous fundamental biological processes such as cellular metabolism, DNA synthesis and neurotransmission.[5] The deficiency of Zn^{2+}ions causes various diseases such as Alzheimer's, Parkinson's diseases, epilepsy regulation disorder in mammalian reproduction, immune system, sense of taste and smell and overall growth of the living body.[6] The zinc is an important constituent in more than 250 metalloenzymes.[7] Cobalt plays a significant role in the metabolism of ferrous and hemoglobin synthesis. The Co^{2+} ions are an important constituent in vitamins.[8] The Co^{2+} shows toxicological effects on human health, including decreased cardiac output, asthma, heart and lung disease.[9] Ni^{2+} is an essential trace ion in organic systems, but the excess accumulation of Ni^{2+} in the body can lead to various diseases such as lung fibrosis, cardiovascular and kidney diseases.[10]

In recent decades, a wide number of efficient chemosensors (ligands) have been developed for the detection of various metal ions in aqueous solution. The type of interaction between chelate and the metal ion is a coordinate bond or host-guest type.[11] Various methods have been used for detection of the metal ions such as rhodamine 6G (R6G) and 8-aminoquinoline (8-AQ) co-modified core/shell $Fe_3O_4@SiO_2$ nanoparticles used for detection of Hg^{2+} and Zn^{2+}ions in aqueous solution,[12] Rhodamine B chemosensor used for detection of Pb^{2+}in acetonitrile,[13] azadiene-pyrene derivative for Hg^{2+} in aqueous acetonitrile solution,[14] (E)-2-(5-((2-carbamothioylhydrazono)methyl)-6-hydroxy-3-oxo-3*H*-xanthen-9-yl)benzoic acid for the detection of Cd^{2+} ions in aqueous solution,[15] *N*-(1,10-phenanthrolin-5-yl)-2,2-diphenylacetamide for selective detection of Fe^{3+} in an aqueous medium,[16] 8-hydroxyquinoline based graphene oxide for detection of Zn^{2+} in aqueous media,[17] cyclometalated platinum(II) bipyridylacetylide complex for Mg^{2+} in acetonitrile,[18] rhodamine-based compound for Pd^{2+}in pure water,[19] and for highly selective detection of Ag(I) ions.[20]

The syntheses of chemosensors are reported in the literature by various methods from readily available starting materials such as water meditated synthesis of CF_1-CF_3 and use for detection of CN^{-1}.[21] Ultrasound-assisted synthesis of diphenylamine-based Schiff base used in the detection of copper(II) ion in aqueous solution,[22] microwave-assisted synthesis of graphitic carbon nitride quantum dots[23] and photoluminescent carbon dots synthesis using starch (*Tapioca Sago*) via solution method at mild condition[24] and possess great applications in various fields such as environmental,[25] forensic,[26] and the biological sciences.[27]

Herein, we develop an ultrasound-assisted new method for the synthesis of amide-based chemosensor using

DOI: http://dx.doi.org/10.17628/ecb.2019.8.212-215

diethylenediamine and benzoyl chloride. Ultrasound waves accelerate the rate of reaction by cavitation and nebulization phenomenon. The cavitation helps to create a development of implosive collapse of bubbles in a liquid. Nebulization phenomenon helps in the creation of mist from ultrasound passing through a liquid and impinging on a liquid-gas interface.[28]

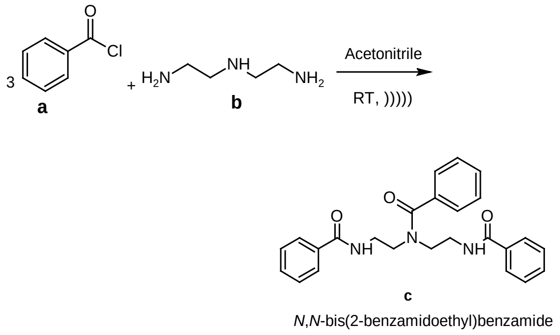

Materials and methods

All chemicals were purchased from Sigma Aldrich and used without further purification. UV spectrophotometric analysis was carried out using UV-VIS Perkin Elmer, lambda scan-35 system. FT-IR analysis was done on a BRUKER instrument having OPUS software of version 7.0.129.

Procedure for synthesis of amide-based chemo-sensor

In 25 mL round bottom conical flask benzoyl chloride (5.00 mmol), diethylenetriamine (10.00 mmol) and 1-2 mL acetonitrile were taken and kept in ultrasonication bath at room temperature for 10 minutes. The reaction mixture was poured into ice-cold water, and the precipitate of chemosensor was separated by simple filtration. Residue allowed drying at room temperature and dry white crystalline powder compound is used as chemosensor in aqueous ethyl alcohol.

Procedure for preparation of pH 10 buffer solution

For 10 ml: pH 10 buffer was prepared by taking 0.7 g of NH_4Cl, and 5.68 mL NH_3 solution in 10 mL distilled water in a conical flask.

Results and discussion

In the present work, we developed a new method for the synthesis of amide-based chemosensor ((7*E*)-N^{1}-benzylidene-N^{2}-((*E*)-2-(benzylideneamino)ethyl)ethane-1,2-diamine) using diethylenetriamine and benzoyl chloride under ultrasound irradiation. The absorbance in the UV-VIS analysis of Co(II) ion solution in aqueous ethanol for 100, 200, 300, 400, 500, 600, 700, 800, 900 and 1000 ppm are illustrated in Figure 2. It was observed that as the concentration of a metal ion in solution was increased, the absorbance was increased. It helps to find out the concentration of a metal ion in an unknown solution by using a standard calibration curve. Mercury (Hg^{2+}), nickel (Ni^{2+}) and copper (Cu^{2+}) show excellent absorbance in the UV-VIS analysis. It was observed that metal ions form stable complexes with chemosensor and show visible color change or change in color intensity of aqueous solution. In UV-VIS analysis, absorbance was increased with respect to concentration and it validates the Lambert-Beer's Law.

The FT-IR spectroscopic technique was used to predict the functional group of chemosensor and metal-complex of chemosensor with the help of stretching frequencies. These results are illustrated in Table 1. The probable interaction of chemosensor with metal ions shows that it forms a stable coordination complex with a metal ion (a predicted structure is given in Figure 1). The synthesized amide-based derivative probably acts as a tridentate ligand showing chromophoric nature with the given metal ions and acts as chemosensor.

Table 1.FT-IR analysis of chemosensor and samples

No.	Sample / Compound	Frequencies, cm^{-1}	Assigned group
1.	Chemosensor	3623, 3750 2982 1700 1647, 1546 1280 1046	N-H C-H (aromatic) C=O C=C (aromatic) C-C C-N
2.	Chemosensor after reacting with 1% Cu.	2946 2876 1746 1656, 1621,1546 3231, 3456	C-H C-H (Aliphatic) C=O C=C (Aromatic) N-H
3.	Chemosensor after reacting with 1% Hg.	2972 1748 1648 1195 1317 3234-3496	C-H (Aliphatic) C=O C=C (Aromatic) C-N C-O N-H
4.	Chemosensor after reacting with 1% Ni	951 2892 3365	N-Ni^{2+} C-H (Aromatic) N-H

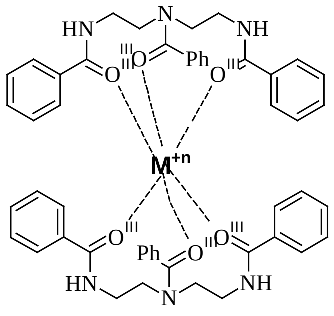

Figure 1. Amide based chemosensor forms coordination complex with metal ions

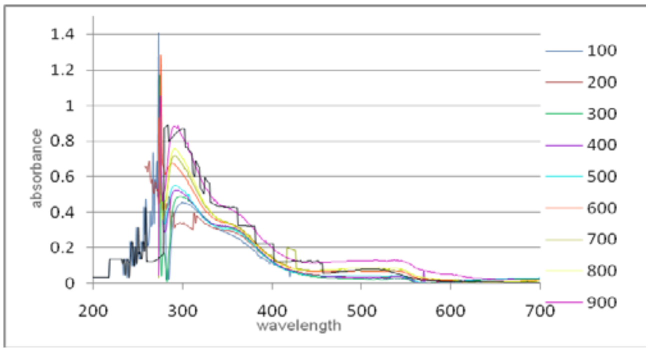

Figure 2. UV analysis of Co^{2+} dilutions with chemosensor (100-1000 ppm)

Conclusion

We developed a simple, efficient and eco-friendly method for the synthesis of amide-based chemosensor from commercially available material. We studied the application of chemosensor for qualitative and quantitative analysis of metal ions in a various extracted solution using UV-VIS spectroscopy techniques. This chemosensor helps in the preliminary analysis and detection of Hg^{2+}, Co^{2+}, Ni^{2+}, Cu^{2+} metal ions in aqueous and spiked solutions. This chemosensor has excellent application in forensic chemistry and toxicology to detect the metal poisoning cases.

Acknowledgment

We are thankful to the Department of Forensic Chemistry and Toxicology, Government Institute of Forensic Science, Aurangabad for the permission to use laboratory and sophisticated instrumentation facility. Authors are especially thankful to Dr. S. G. Gupta (Director, Government Institute of Forensic Science, Aurangabad) for support and permitting us to use the sophisticated instrumentation facility. □

References

[1]Lee, S., Choi, I., Hong, S., Yang, Y.I., Lee, J., Kang, T., Yi, J., Highly selective detection of Cu^{2+} utilizing specific binding between Cu-demetallated superoxide dismutase 1 and the Cu^{2+} ion *via* surface plasmon resonance spectroscopy, *Chem. Commun*., **2009**, *41*, 6171-6173. doi: 10.1039/b910666a

[2]Zhang, X., Xiao, Y., Qian, X., A Ratiometric Fluorescent Probe Based on FRET for Imaging Hg^{2+} Ions in Living Cells, *Angew. Chem. Int. Ed*., **2008**, *47*, 8025. doi.org/10.1002/anie.200803246

[3]Li, L. Q., A Colorimetric and Fluorescent Chemosensor for Cu^{2+} Detection in Aqueous Solution, *Synth. React Inorg. Metal-Org. and Nano-Metal Chem*., **2016**, *46*, 1854-1856. doi.org/10.1080/15533174.2015.1137077

[4]Que, E. L., Domaille, D. W, Chang, C. J., *Metals in neurobiology: Probing their chemistry and biology with molecular imaging. Chem Rev*, **2008**,*108*, 1517-1548.doi: 10.1021/cr078203u

[5]Feng, J., Shao, X., Shang, Z., Chao, J., Wang, Y., Jin, W., A new biphenylcarbonitrile based fluorescent sensor for Zn^{2+} ions and application in living cells, *Chem. Res. Chin. Univ.*, **2017**, *33*, 695-701. doi: 10.1007/s40242-017-7084-z

[6]Patra, C., Bhanja, A. K., Sen, C., Ojha, D., Chattopadhyay, D., Mahapatraa, A., Sinha, C., Imine-functionalized thioether Zn(II) turn-on fluorescent sensor and its selective sequential logic operations with $H_2PO_4^-$, DFT computation and live cell imaging, *RSC Adv*., **2016**, *6*, 53378-53388. doi: 10.1039/C6RA07089B

[7]Bertini, I., Gray, H. B., Lippard, S. J., Valentin, J. S., *Bioinorg. Chem.*, **1994**, University Science Books, Mill Valley, CA (USA). ISBN 0-935702-57-1

[8]Park, G. J., Na, Y. J., Jo, H. Y., Lee, S. A., Kim, C., A colorimetric organic chemo-sensor for Co^{2+} in a fully aqueous environment, *Dalton Trans*., **2014**, *43*, 6618-6622. doi: 10.1039/C4DT00423J

[9]Sun, J., Ye, B., Xia, G., Wang, H. M., A multi-responsive squaraine-based "turn on" fluorescent chemosensor for highly sensitive detection of Al^{3+}, Zn^{2+} and Cd^{2+} in aqueous media and its biological application, *Sens. Actuators B: Chem.*, **2016**, *223*, 234-240. doi.org/10.1016/j.snb.2017.03.134

[10]Liu, X., Lin, Q., Wie, T.-B., Zhang, Y.-M., A highly selective colorimetric chemosensor for detection of nickel ions in aqueous solution, *New J. Chem*., **2014**, *38*, 1418-1423. doi: 10.1039/C3NJ01403G

[11]Shahabuddin, M., Ashfaque, A. B., Asif, A. B., A new calix[4]arene Schiff base sensor for Hg^{2+} and Au^{3+}, *J. Iran. Chem. Soc*, **2016**, *13*, 2275-2282. https://doi.org/10.1007/s13738-016-0946-3

[12]Yao, G., Guowen, M., Meiling, W., Qing, H., Chuhong, Z., Zhulin, H., R6G/8-AQ co-functionalized $Fe_3O_4@SiO_2$ nanoparticles for fluorescence detection of trace Hg2+ and Zn^{2+} in aqueous solution, *Sci. China Mater*, **2015**, *58*, 550-558. doi: 10.1007/s40843-015-0071-0

[13]Ji, Y. K., Yun, J. J., Yoon, J. L., Kwan, M. K., Mi, S. S., Wonwoo, N., Juyoung, Y., A Highly Selective Fluorescent Chemosensor for Pb^{2+}, *J. Am. Chem. Soc.*, **2005**, *127*, 10107-10111. doi: 10.1021/ja051075b

[14]Zhou, Y., Zhu, C.-Y., Gao, X.-S., You, X.-Y., Yao, C., Hg^{2+}-Selective Ratiometric and "Off−On" Chemosensor Based on the Azadiene−Pyrene Derivative, *Org. Lett*., **2010**, *12*, 2566-2569. doi: 10.1021/ol1007636

[15]Liu, W., Xu, L., Sheng, R., Wang, P., Li, H., Wu, S., A Water-Soluble "Switching On" Fluorescent Chemosensor of Selectivity to Cd^{2+}, *Org. Lett*., **2007**, *9*, 3829-3832. doi: 10.1021/ol701620h

[16]Nadeem, S., Shah, M. R., Khan, B., Hoda, N., Topel, Ö., Supramolecular chemosensor for selective detection of iron in aqueous medium, *Supramol. Chem.*, **2013**, *25*, 798-805. doi.org/10.1080/10610278.2013.804186

[17]Eftekhari-Sis, B., Rezazadeh, Z., Akbari? A., Amini, M., 8-Hydroxyquinoline Functionalized Graphene Oxide: an Efficient Fluorescent Nanosensor for Zn2+ in Aqueous Media, *J. Fluoresc.*, **2018**, 28, 1173-1180. doi.org/10.1007/s10895-018-2281-9.

[18]Yang, Q.-Z., Wu, L.-Z., Zhang, H., Chen, B., Wu, Z. X., Zhang, L. P., Tung, C.- H., A Luminescent Chemosensor with Specific Response for Mg^{2+}, *Inorg. Chem.*, **2004**, *43*, 5195-5197.doi: 10.1021/ic049815p

[19]Wang, M., Liu, X., Lu, H., Wang, H., Qin, Z., Highly Selective and Reversible Chemosensor for Pd^{2+} Detected by Fluorescence, Colorimetry, and Test Paper, *ACS Appl. Mater. Interfaces*,**2015**, *7*, 1284-1289. doi: 10.1021/am507479m

[20]Coskun, A., Akkaya, E. U., Ion Sensing Coupled to Resonance Energy Transfer: A Highly Selective and Sensitive Ratiometric Fluorescent Chemosensor for Ag(I) by a Modular Approach, *J. Am. Chem. Soc*., **2005**, *127*, 10464-10465. doi: 10.1021/ja052574f

[21]Lin, Q., Fu, Y.-P., Pei, C., Wei, T. B., Zhang, Y.-M., Rational design, green synthesis of reaction-based dual-channel chemosensors for cyanide anion, *Tetrahedron Letters*, **2013**, *54*, 5031-5034. doi.org/10.1016/j.tetlet.2013.07.022

[22] Parsaee, Z., Haratipour, P., Lariche, M. J., Vojood, A., A novel high-performance nano chemosensor for copper (II) ion based on an ultrasound-assisted synthesized diphenylamine-based Schiff base: Design, fabrication and density functional theory calculations, *Ultrasonics Sonochem.*, **2018**, *41*, 337-349. doi.org/10.1016/j.ultsonch.2017.09.054

[23] Li, H., Shao, F. Q., Huang, H., Feng, J.-J., Wang, A.-J., Eco-friendly and rapid microwave synthesis of green fluorescent graphitic carbon nitride quantum dots for vitro bioimaging, *Sensors Actuators B*, **2016**, *226*, 506-511. doi.org/10.1016/j.snb.2015.12.018

[24] Basu, A., Suryawanshi, A., Kumawat, B., Dandia, A., Guin, D., Ogale, S. B., Starch (Tapioca) to carbon dots: an efficient green approach to an on-off–on photoluminescence probe for fluoride ion sensing, *Analyst*, **2015**, *140*, 1837-1841. doi:10.1039/C4AN02340D

[25] Lieberzeit, P. A., Dickert, F. L., Chemosensors in environmental monitoring: challenges in ruggedness and selectivity, *Anal. Bioanal. Chem.*, **2009**, *393*, 467. DOI:10.1007/s00216-008-2464-3

[26] Yilmaz, E., Garipcan, B., Patra, H. K., Uzun, L., Molecular Imprinting Applications in Forensic Science, *Sensors*, **2017**, *17*, 691-695. https://doi.org/10.3390/s17040691

[27] Jung, H.-S., Ko, K. C., Kim, G.-H., Lee, A.-R., Na, Y.-C., Kang, C., Lee, J. Y., Kim, J. S., Coumarin-Based Thiol Chemosensor: Synthesis, Turn-On Mechanism, and Its Biological Application, *Org. Lett.*, **2011**, *13*, 1498-1501. https://doi.org/10.1021/ol2001864

[28] Bang, J. H., Suslick, K. S., Applications of Ultrasound to the Synthesis of Nanostructured Materials, *Adv. Mater.*, **2010**,*22*, 1039-1059. doi.org/10.1002/adma.200904093

This paper was presented at the "*International Symposium on Exploring New Horizons in Chemical Sciences*", January 10–12, **2019**, Aurangabad, India (ENHCS–2019).

Received: 11.03.2019
Accepted: 14.07.2019.

EFFECT OF SILVER ION REDUCTION ON ELECTRICAL MODULUS OF CHITOSAN-SILVER TRIFLATE SOLID POLYMER ELECTROLYTE MEMBRANE

Soran Kamal[a] and Sleman Qadir[a]

Keywords: silver; electrical modulus; polymer electrolyte; chitosan; silver triflate

Utilizing impedance spectroscopy, chitosan-based solid polymer electrolyte containing CF_3SO_3Ag was investigated for their electric modulus properties. Using the highest conductivity sample, the lowest conductivity relaxation time (τ_σ) was determined. The high capacitivity of the material is shown by the electrical modulus of the real part. A non-Debye type relaxation is predicted by the asymmetric peak of electric modulus's imaginary part (M''). Utilizing Argand plot, a deformed arc for the relaxation times distribution is demonstrated. Silver nanoparticles formed from silver ions causes a rise in the values of M' and M'' above 358 K. The ultraviolet-visible (UV-vis) absorption and complex impedance of silver nanoparticles in chitosan-silver triflate solid electrolyte are temperature dependent. Transmission electron microscopy (TEM) confirmed the silver nanoparticles formation. The dynamical relaxation process for a particular composition is proven by the scaling behavior of M'' spectra to be independent of temperature. The conductivity relaxation is shown by a β exponent to be non-exponential.

* Corresponding Authors
E-Mail: soran3979@gmail.com
[a] KSCIEN Organization for Scientific Research, Hamdi Street, Sulaimani, Iraq.

Introduction

Very intriguing classes of solid-state coordination compounds are polymer electrolytes that utilize solid but flexible membranes for ionic conductivity.[1] Because of the attractive interaction between cations and chains, chain polymers can act as solvents for certain salts if they have electronegative atom (nitrogen or oxygen) in their repeating units.[2] Chitosan polymers contain both N and O atoms in their chains[3] are used as solid electrolytes in electrochromic displays, sensors, fuel cells and batteries.[4,5] Despite the intensive studies, the mechanism for their conductivity is still not clarified completely.[6] The amorphous phase is the main conductive phase, despite the coexistence of crystalline and amorphous phases.[7] Little is understood about the coupling between ion transport and polymer segmental relaxation in polymer electrolytes and could be the key for new discoveries.[8]

In the polymer electrolytes, both dipoles and charge species affect the relaxation dynamic and frequency dependent conductivity.[9] Electric modulus formalism M'' can be used as an environment for studying relaxation dynamics, specifically dielectric relaxation.[10] M'' displays a pronounced peak, leading to modulus representation and associating the extent of conductivity with time scale τ.

Despite the well establishment of relations between the various quantities, yet there is still debate on modulus representation.[11] When the electric displacement is constant, from the physical viewpoint, the relaxation of electric fields in the material is correspondent to the electrical modulus.[12] Emphasizing small features at high frequencies and suppressing the high signal intensity associated with electrode polarization is the main benefit of modulus representation.[11] Therefore, studying relaxation times and conductivity in polymers and ionic conductors can be achieved through electric modulus spectra.[13]

In the chitosan-silver triflate polymer electrolyte thin film preparations, commercial chitosan was used as a base polymer containing amine and hydroxyl functional groups and suitable for solid polymer electrolyte preparation.[14] Silver salts like $AgSbF_6$, CF_3SO_3Ag, $AgBF_4$ and $AgClO_4$ were tested in polymer hosts like and poly(vinylpyrrolidone) (PVP), poly(ethylene oxide) (PEO) and poly(2-ethyl-2-oxazoline)(POZ) to make silver-based polymer electrolytes.[15,16] Olefin transport is facilitated essentially by nitrogen and oxygen atoms contained within polar polymer chains, and silver metal particles were formed due to the reduction of silver ions.[17,18]

Due to these properties, the effect of silver nanoparticle reduction from silver ions on the properties of electrical modulus of chitosan-silver triflate solid electrolyte is studied in this paper over a wide range of temperature and frequency.

Experimental

Solid polymer electrolyte (SPE) thin film preparation

Silver triflate (CF_3SO_3Ag) (Fluka, ε99 purity, Germany, CAS No. 2923-28-6) and chitosan from crab shells (ε75 % deacetylated, Sigma Aldrich, USA, CAS No. 9012-76-4) were used as raw materials. Solution cast technique with the solvent being acetic acid (1 %) is used for the preparation of solid polymer electrolyte (SPE) films. Chitosan (1 g) is dissolved in acetic acid solution and fixed in the current system. Varying amount of silver triflate (CF_3SO_3Ag) ranging from 2 to 10 wt. % in steps of 2 wt. % is added to this system to adjust different compositions of chitosan-

DOI: http://dx.doi.org/10.17628/ecb.2019.8.216-223

silver triflate electrolyte in weight percent ratios; 98:2, 96:4, 94:6, 92:8 and 90:10 for chitosan: CF_3SO_3Ag and 100:0 for pure chitosan acetate. To obtain a homogenous solution, the mixture is continuously stirred until said result is obtained. In room temperature, the solutions are left to dry in different Petri dishes after casting, in order to form the films, then further drying is done by transferring into desiccators. The result is a solvent-free and mechanically stable film.

Complex impedance measurement

Characterization of the materials electrical properties is done through the complex impedance spectroscopy. Small discs of 2 cm diameter are made from the SPE films, and to ensure proper electrical contact between the sample and electrodes, two clean stainless steel and circular shaped electrodes are used under spring pressure. This solves the problem of air interstices between the electrodes and the sample interface. HIOKI 3531 Z Hi-tester (made in Japan, No.1036555) is used to measure the impedance of films in the frequency range from 50 to 1000 kHz. The imaginary and real parts of the impedance is calculated and measured by the software. Using b equations below, the real (M') and imaginary (M'') parts of complex electric modulus (M^*) is evaluated by the use of the real (Z') and imaginary (Z'') part of complex impedance (Z^*) [19]:

$$M^* = 1/\varepsilon^* = M' + jM'' = j\omega C_0 Z^*$$

$$M' = \frac{\varepsilon'}{\varepsilon'^2 + \varepsilon''^2} \quad \text{and} \quad M'' = \frac{\varepsilon''}{\varepsilon'^2 + \varepsilon''^2}$$

$$Z^* = Z' - jZ''$$

where

C_0 is the vacuum capacitance and given by $\varepsilon_0 A/l$,

A is the area of the film,

l is the thickness and

The angular frequency is represented by ω and is equal to $\omega = 2\pi f$; the applied field's frequency is f.

UV-Vis and TEM characterization

The absorbance mode of Jasco V-570 UV-Vis-NIR spectrophotometer (Japan, Jasco SLM-468) is used to record the UV spectra of chitosan-silver triflate electrolyte films. An LEO LIBRA (Germany, 120 EFTEM, accelerating voltage 120 kV) TEM instrument was used. The excess solution was removed by a filter paper from the dried chitosan-silver triflate electrolyte solution placed on a carbon-coated copper grid at room temperature.

Results and discussions

Concentration dependence of M″ spectra

The M'' spectra frequency dependencies for compositions with different silver triflate content at 303 K are shown in Figure 1. In the highest conducting sample could be observed higher frequencies for maximum M'' peaks. Possibly due to polar group relaxations especially at low frequency, pure chitosan and chitosan-silver triflate (98:2) may show more than one peak. At higher salt concentrations, because of the motion and high free charge carrier concentration within the material, these peaks are disappeared. Consequently, the low-frequency relaxation can be hidden due to a high DC conductivity that is produced.

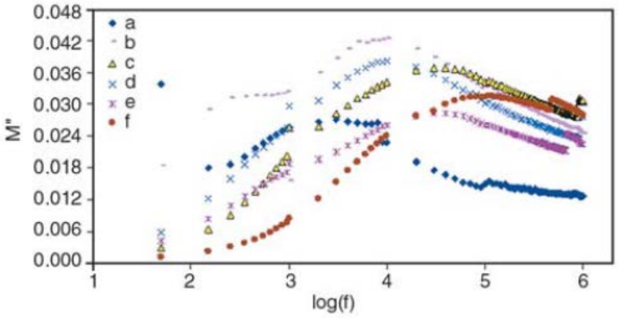

Figure 1. Concentration dependence of M'' for (a) pure chitosan acetate (100:0), (b) 98:2, (c) 96:4, (d) 94:6, (e) 92:8 and (f) 90:10 for chitosan: CF_3SO_3Ag at 303 K.

Broadening of the peaks suggests a non-Debye type relaxation, representing the conductivity relaxation peaks distribution of the free charges.[20] As conductivity increases, the relaxation times decrease and causing shifting to higher frequencies.[21] Through the relation $2\pi f_{max} = 1/\tau_\sigma$, we can calculate the conductivity relaxation times, were f_{max} is a frequency corresponding to M''_{max} and τ_σ is the conductivity relaxation time. Figure 2 shows silver triflate concentration function as a variation of τ_σ as the salt concentration increases up to 4 wt. % CF_3SO_3Ag, the conductivity relaxation ties decrease. We can deduct from the results, especially at the 4-8 wt. % concentration that there is a competition between the ion associations and dissociations — a charge carriers concentration increases from 8 wt. % CF_3SO_3Ag to 10 wt. % CF_3SO_3Ag explains the significant drop in conductivity relaxation times, i.e., as the number of mobile charge carriers increases, the conductivity increases.

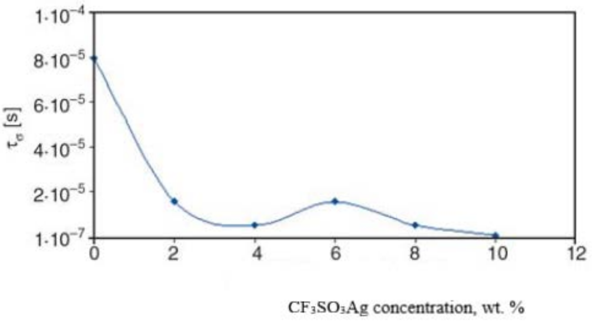

Figure 2. Concentration dependence of conductivity relaxation time (τ_σ) at 303 K

M′ and M″ frequency dependence at selected temperatures

The imaginary and the real part's frequency dependence of the complex modulus for the sample with the highest conductivity (90:10) at various temperatures are shown in Figure 3 and 4. Equations given were used to calculate the imaginary and real parts of the complex modulus.

Using the representation of electrical modulus (*M**), the conductivity behavior in regards to conductivity relaxation time can be interpreted conveniently. Ionic conductivity analysis is commonly done by the representation of *M** through ionic process association with conductivity relaxation time.[22] *M*′ are very small at lower frequencies, as illustrated by Figure 3, the electrode polarization is close to zero thus can be neglected.[23,24]. At higher frequency, *M*′ increases until reaching the maximum value of M_∞ due to the wide range of relaxation process frequencies.[25] The spread of conductivity relaxation over a range of frequencies explains the observed dispersion and pointing to the occurrence of relaxation time and the presence of a loss of peak at the same time in the imaginary part diagram of electric modulus versus frequency. ε′ in complex permittivity (ε*) is equivalent to *M*′ in complex electric modulus (*M**) and this explains the peak absence in *M*′ diagram, i.e., the capability of the material for energy storage is represented by *M*′. The charge carriers and mobility of the polymer increase with increasing the temperature and due to this, the *M*′ values are decreased.

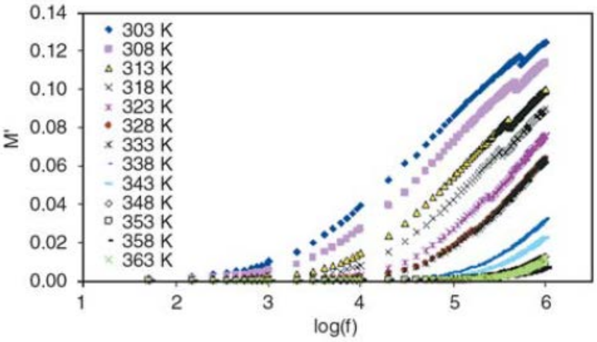

Figure 3. Frequency dependence of *M*’ at different temperatures for chitosan-silver triflate=90:10 composite

With increasing the temperature, the orientation of molecular dipoles and charge carriers become easier. It is possible that the electrode polarization effect with its large value of capacitance causes *M*″ to exhibit low values at low frequencies.[26] A large amount of charge carriers are accumulated on the interface of electrode/solid polymer electrolyte. The peaks can be seen at high frequencies (Figure 4). The non-Debye behavior is illustrated by the asymmetric and board peaks on both sides of maxima. The region on the right of the peak are carriers that are mobile on short distances and are confined to potential walls, while the region to the left of the peak is carriers that are mobile over a long distance.[24]

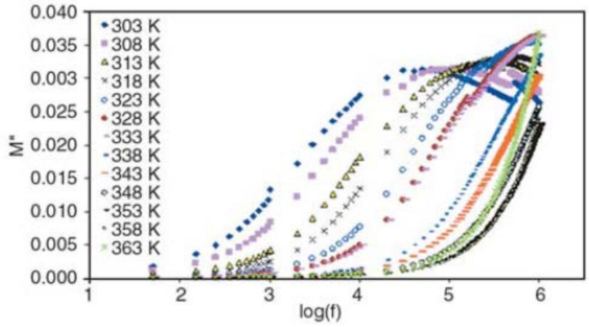

Figure 4. Frequency dependence of *M*″ at different temperatures for chitosan-silver triflate (90:10) composite

Experimental frequency limitation explains the disappearing of the *M*″ peaks at higher temperatures. The formation of silver nanoparticles from the reduction of silver ions contributes to the rise of both *M*′ and *M*″ above 358 K. The function of temperature at a fixed frequency can be used to study *M*′ and *M*″ as a way for studying silver ion reduction to silver nanoparticles.

The best conductivity relaxation time of ions (τ_σ) is the relaxation frequency associated with the peak. Figure 5 demonstrates the relationship of reciprocal temperature and log(f_{max}). The activation energy (Arrhenius behavior), E_a = 1.16 eV.

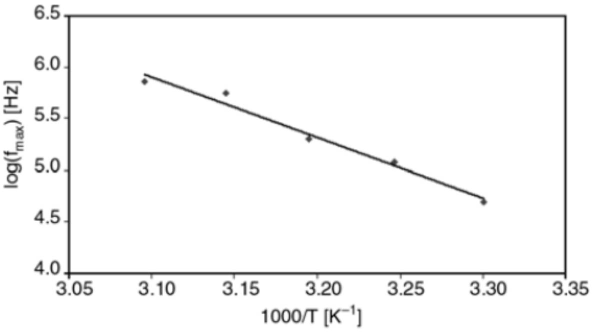

Figure 5. Temperature dependence of relaxation frequency

The rise in the mobility of ionic carriers with rising temperature causes a reduction in relaxation time. The points form almost a straight line, the regression value R^2 is 0.996.

Argand plots analysis

In polymer electrolytes, the nature of the relaxation process can be studied by Argand plot demonstration. The dependence of Argand plot on temperature is shown in Figure 6.

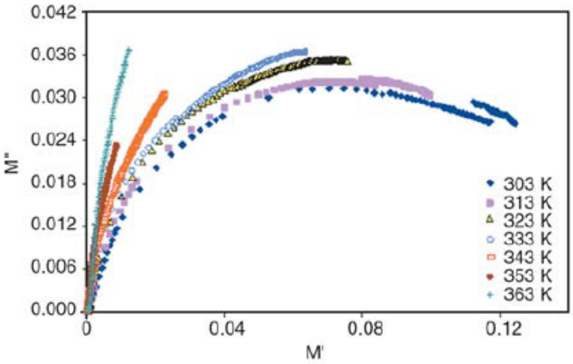

Figure 6. Argand plots for chitosan-silver triflate (90:10) at different temperatures

It can be concluded that the Debye model (single relaxation time) fails to explain the half semicircle curves of Argand plot shown in Figure 6. In this situation, especially in polymers to understand the experimental data, a distribution of relaxation time becomes mandatory.

The possible reasons for this distribution type are space charge polarization, hopping, the ellipsoidal shape of polar groups and the presence of inhomogeneity.[27] At lower temperatures, the Argand plot shows deformed arcs with centers localized below the horizontal axis. The electric relaxation of material corresponds with this position of the centers as well as distribution and intercorrelation of activation energy and relaxation time.[28] There is a shift in Argand curves when the temperature rises (Figure 6). This can be explained with increasing of ionic mobility with the increased conductivity resulting from risen temperature and both Z' and Z'' increase, subsequently. At 363 K, the resistance within the sample increases, since a large amount of silver nanoparticles form from silver ions reductions, causing an increase on M''–M' curves.

The dependence of M′ and M″ on t

he temperature shown in Figure 7a and 7b. Until 358 K due to a rise of ionic conductivity, M' and M'' decrease as the temperature rises because of the dominance of silver ions. However, above 358 K, a large amount of silver ions transform into silver nanoparticles causing M' and M'' to increase with rising the temperature. The ionic motion is hindered by the increase of resistance within the sample caused silver nanoparticles.

The complex impedance plots can detect the presence of silver nanoparticles within the sample. Phase transitions, interfacial effects in polymers and complex systems, molecular mobility and conductivity mechanisms can also be efficiently studied by electrochemical impedance spectroscopy.[29]

Figure 8 supports the above statement; the complex impedance plots at different temperatures explain the increase of M' and M''. The electrode surface polarization phenomena (i.e., tilted spike) is often separated from the bulk material (i.e., depressed semicircle) in the complex impedance plots (Z'' *vs.* Z').[30]

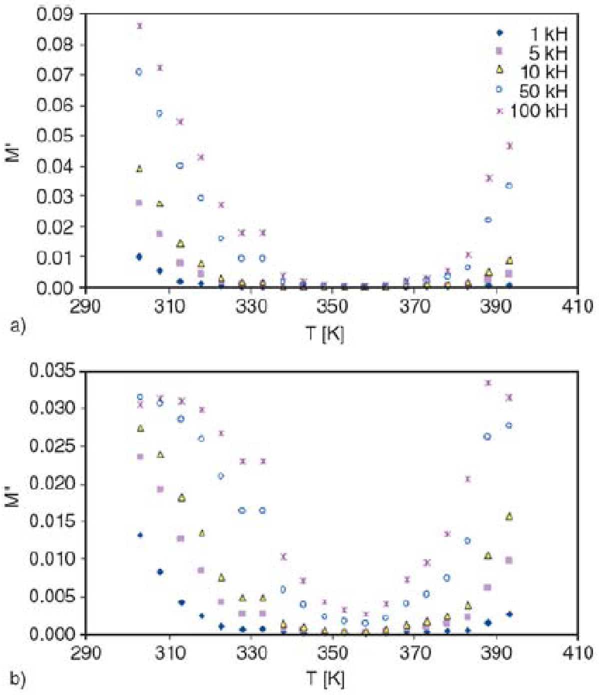

Figure 7. Temperature dependence of (a) M' and (b) M'' at selected frequencies for chitosan-silver triflate (90:10) composite

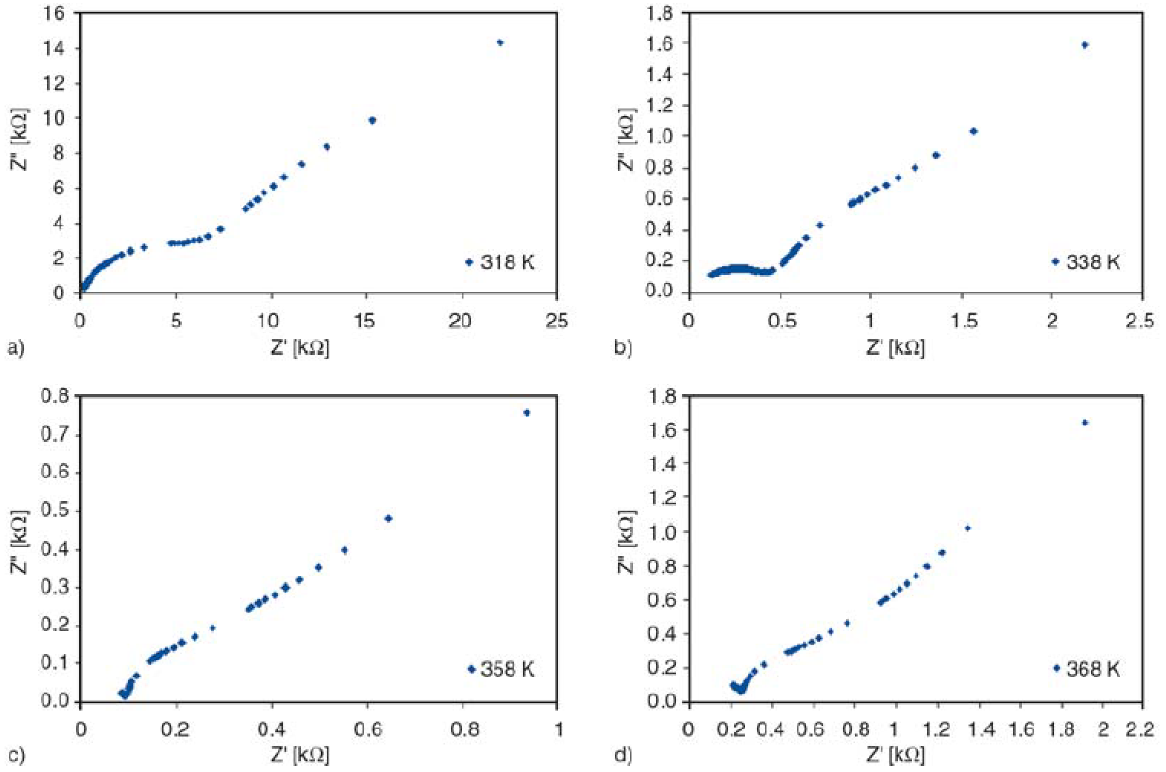

Figure 8. Complex impedance of chitosan-silver triflate (90:10) composite at selected temperatures

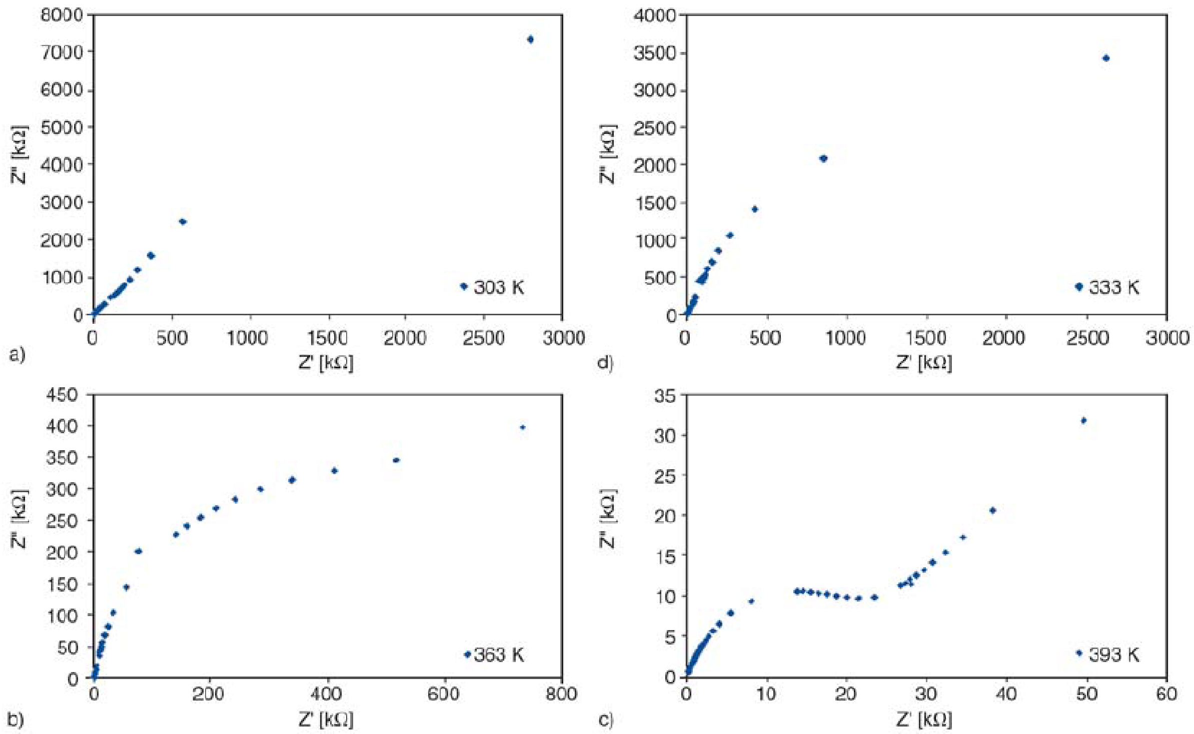

Figure 9. Complex impedance plots of pure chitosan at selected temperatures

The free charges are building up in the interface of the electrode surfaces and the electrolyte form an electric double layer (EDL) capacitance that results in the formation of electrode polarization phenomena (tilted spike).[30,22] The silver nanoparticles act as grain boundaries causing second semicircles to appear at different temperatures (Figure 8). It can be concluded that the silver nanoparticles and silver ions compete. As the temperature rises from 303 to 358 K, the bulk resistance decreases, i.e., silver ions are dominant and the system behaves as an ionic conductor. However, when the temperature passes 358 K, the bulk resistance increases since more silver nanoparticles are formed from silver ions. Subsequently, both M' and M'' increase since the conduction mechanism and overall polarization decrease because of the decline in silver ion amounts. Z' and Z'' increase above 358 K. At this point, a noncomposite behavior seems to be appeared due the polymer electrolyte rather than ionic behavior. On the other hand, in pure chitosan (Figure 9), the second semicircles cannot be seen.

The complex impedance plot of pure chitosan is shown in Figure 9 at different temperatures. The bulk resistance of chitosan-silver triflate (90:10) solid electrolyte is lower than that of pure chitosan. Also, there is a continuous decrease in pure chitosan's bulk resistance as the temperature increases up to 393 K. It is a difference comparing that to the Z''–Z' plot of chitosan-silver triflate (90:10) solid electrolyte. Another observation would be that pure chitosan in its Z''–Z' plot does not manifest second semicircles as temperature changes.

Specific UV-vis absorption band can be seen for silver nanoparticles and their clusters in the ultraviolet-visible region.[31] The UV-Vis absorption spectra at temperature 303 K for chitosan-silver triflate (90:10) solid electrolyte and pure chitosan are shown in Figure 10.

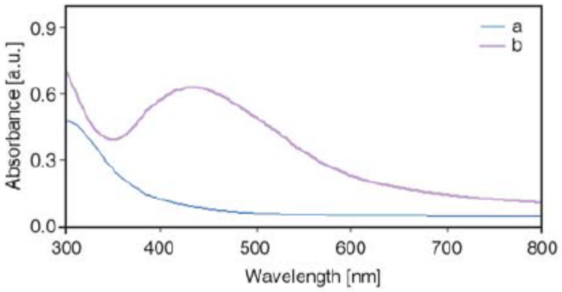

Figure 10. UV-Vis absorption spectra of (a) pure chitosan and (b) chitosan- CF_3SO_3Ag (90:10) composite at 303 K.

The chitosan-silver triflate (90:10) solid electrolyte has a broad absorption peak from 400 to 500 nm with maximum being at 426 nm, mainly due to the surface plasmon band of silver nanoparticles. Pure chitosan has no specific absorption peak within this wavelength range. The concentration of the silver nanoparticles corresponds with the height of the peak.[32,33]

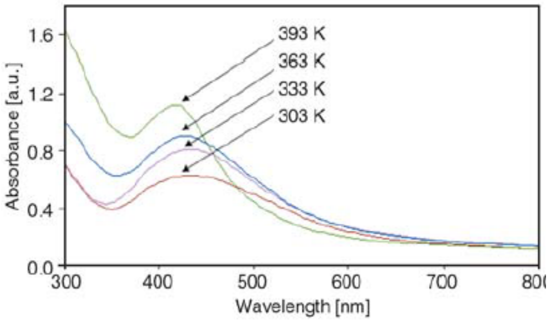

Figure 11. UV-Vis absorption spectra of chitosan- CF_3SO_3Ag (90:10) composite at different temperatures

The UV-Vis absorption spectra of chitosan-silver triflate (90:10) solid electrolyte at different temperatures is shown in Figure 11. As the temperature increases from 303 K to 393 K, the peak heights increase from 0.61 to 1.2. It shows that at high temperatures, more rapid conversion of silver ions to silver nanoparticles occurs.[34] It has been reported that the silver ion reduction can occur in hydroxyl, carboxyl and imide group-containing polymers.[35,36] The color change of solid membranes from yellow to dark brown is another indicator of silver nanoparticle formation. Similar behavior for PVP-silver salt electrolyte was mentioned by Kang *et al*.[37] Interacting electromagnetic field causes the free conduction electrons to oscillate (surface plasmon resonance (SPR)).[38] The intense color in the visible spectrum can only be seen in electrodes with plasmon resonance since they have free electrons.[39]

The presence of silver nanoparticle was confirmed with transmission electron microscopy (TEM). The silver nanoparticles within chitosan- CF_3SO_3Ag (90:10) solid electrolyte can be seen in Figure 12. It can be seen that they are agglomerated and dispersed. When the repulsion energy is lower than the attraction energy between the particles, it leads to particle agglomeration.[40]

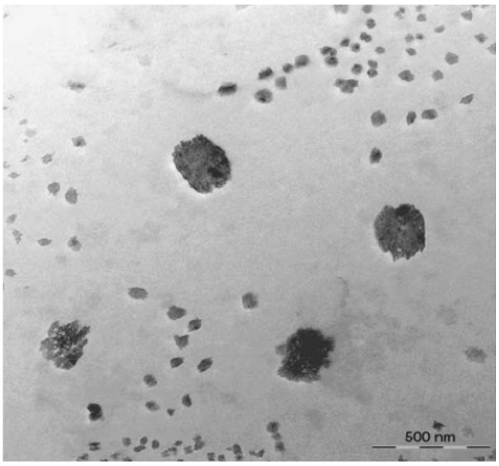

Figure 12. TEM micrograph of silver nanoparticles for chitosan-silver triflate (90:10) composite at room temperature

As far as we know, change in properties of solid polymer electrolytes (SPE) by the effect of silver ion reduction to silver nanoparticles is reported for the first time.

Scaling behavior of M".

More information can be obtained on the effect of charge carrier concentration, structure, and temperature on relaxation dynamics by studying the scaling of electric modulus.[41] Figure 13 shows the electric modulus of chitosan-silver triflate (90:10) as its imaginary part is scaled at different temperatures. The parameters of M'' and f are scaled according to M''_{max} and f_{max}, respectively.

A single master curve is formed by merging of all the modulus spectra (Figure 13). For the particular compositions, the dynamical relaxation is independent on temperature.[42] Deviation from Debye behavior can be seen from the dielectric relaxation processes evidenced by the asymmetric plot shape and the non-symmetric distribution of relaxation times.[43] A clear non-symmetric plot can be seen for the normalized modulus in Figure 13, in accordance with the non-exponential behavior of electrical functions.[44]

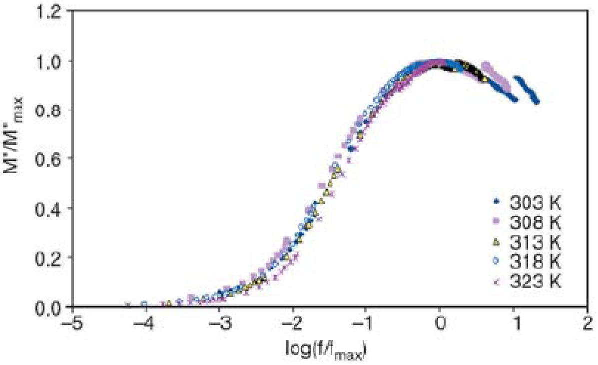

Figure 13. Scaling of M'' for chitosan-silver triflate (90:10) composite at different temperatures

The deviation from Debye relaxation can be shown from the exponent β. The typical Debye behavior is 1.14 decades, while in the chitosan:CF_3SO_3Ag (90:10) composite full-width half height (FWHH) is nearly 2 decades. A highly non-exponential conductivity relaxation is concluded from the small value (0.57) of β.[42] Deviation from Debye-type relaxation becomes the more significant the lower the value of β (standard value is $\beta=1$). A practical solid electrolyte has a β value of less than 1.[20]

Conclusions

A solution casting preparation of chitosan-silver triflate electrolytes resulted in composite films. The highest conductivity samples have no shift towards higher frequency in their M'' spectra due to a low number of mobile charge carriers. The systems capacitive nature is demonstrated by the long tail of M' spectra in the low-frequency range. Non-Debye relaxation type can be seen from the broad peaks of M'' spectra. Relaxation times distribution gives a deformed arc shape of Argand plots. A large amount of silver nanoparticles formed from silver ions at higher temperatures causing the increase of M' and M'' values. The presence and growth of silver nanoparticles result in the appearance of the temperature dependence of second semicircles in complex impedance plots. UV-Vis and transmission electron microscopy (TEM) confirmed the formation of silver nanoparticles. A temperature independent nature of the dynamical relaxation processes was demonstrated and a highly non-exponential nature of the conductivity relaxation is concluded from the value of the β exponent.

References

[1] Karan, N. K., Pradhan, D. K., Thomas, R., Natesan, B., Katiyar, R. S., Solid polymer electrolytes based on polyethylene oxide and lithium trifluoro- methanesulfonate (PEO-$LiCF_3SO_3$): Ionic conductivity and dielectric relaxation. *Solid State Ionics*, **2008**, *179*, 689–696. DOI: 10.1016/j.ssi.2008.04.034

[2] Dieterich, W., Dürr, O., Pendzig, P., Bunde, A., Nitzan, A., Percolation concepts in solid state ionics. *Physica A:*

Statistical Theoret. Phys., **1999**, *266*, 229–237. DOI: 10.1016/S0378-4371(98)00597-4

[3] Yahya, M. Z. A., Arof, A. K., Studies on lithium acetate doped chitosan conducting polymer system. *Eur. Polym. J.*, **2002**, *38*, 1191–1197. DOI: 10.1016/S0014-3057(01)00290-7

[4] Bhargav, P. B., Mohan, V. M., Sharma, A. K., Rao, V. V. R. N., Investigations on electrical properties of (PVA:NaF) polymer electrolytes for electrochemical cell applications. *Curr. Appl. Phys.*, **2009**, *9*, 165–171. DOI: 10.1016/j.cap.2008.01.006

[5] Baskaran, R., Selvasekarapandian, S., Kuata, N., Kawamura, J., Hattori, T., Ac impedance, DSC and FT-IR investigations on (x)PVAc-(1–x)PVdF blends with LiClO$_4$. *Mater. Chem. Phys.*, **2006**, *98*, 55–61. DOI: 10.1016/j.matchemphys.2005.08.063

[6] de Jonge J. J., Van Zon A., de Leeuw S. W., Molecular dynamics study of the influence of the polarizability in PEOx-NaI polymer electrolyte systems. *Solid State Ionics*, **2002**, *147*, 349–359. DOI: 10.1016/S0167-2738(02)00056-5

[7] Avellaned, C. O. A., Vieira, D. F., Al-Kahlout, A., Leite, E. R., Pawlicka, A., Aegerter, M. A., Solid-state electrochromic devices with Nb$_2$O$_5$:Mo thin film and gelatin-based electrolyte. *Electrochim. Acta*, **2007**, *53*, 1648– 1654. DOI: 0.1016/j.electacta.2007.05.065

[8] Natesan, B., Karan, N. K., Katiyar, R. S.: Ion relaxation dynamics and nearly constant loss behavior in polymer electrolyte. *Phys. Review E*, **2006**, *48*, 042801/1– 042801/4. DOI: 10.1103/PhysRevE.74.042801

[9] Singh, K. P., Gupta, P. N., Study of dielectric relaxation in polymer electrolytes. *Eur. Polym. J.*, **1998**, *34*, 1023–1029. DOI: 10.1016/S0014-3057(97)00207-3

[10] Chabchoub, N., Khemakhem, H., Ac ionic conductivity investigations on the CsK(SO$_4$)-Te(OH)$_6$ material. J. Alloys Compd., **2004**, *370*, 8–17. DOI: 10.1016/j.jallcom.2003.08.091

[11] Richert, R., The modulus of dielectric and conductive materials and its modification by high electric fields. J. Non-Cryst. Solids, **2002**, *305*, 29–39. DOI: 10.1016/S0022-3093(02)01085-2

[12] Molak, A., Paluch, M., Pawlus, S., Klimontko, J., Ujma, Z., Gruszka, I.: Electric modulus approach to the analysis of electric relaxation in highly conducting (Na$_{0.75}$Bi$_{0.25}$)(Mn$_{0.25}$Nb$_{0.75}$)O$_3$ ceramics. *J. Appl. Phys. D: Appl. Phys.*, **2005**, *38*, 1450–146. DOI: 10.1088/0022-3727/38/9/019

[13] Migahed, M. D., Ishra, M., Fahmy, T., Barakat, A., Electric modulus and AC conductivity studies in conducting PPy composite films at low temperature. *J. Phys. Chem. Solids*, **2004**, *65*, 1121–1125. DOI: 10.1016/j.jpcs.2003.11.039

[14] Majid, S. R., Arof, A. K., Electrical behavior of proton-conducting chitosan-phosphoric acid-based electrolytes. *Physica B: Condensed Matter*, **2007**, *390*, 209–215. DOI: 10.1016/j.physb.2006.08.038

[15] Kim, J. H., Min, B. R., Wong, J., Kang, Y. S., Anomalous temperature dependence of facilitated propylene transport in silver polymer electrolyte membranes. *J. Membrane Sci.*, **2003**, *227*, 197–206. DOI: 10.1016/j.memsci.2003.08.026

[16] Kang, S. W., Kim, J. H., Won, J., Char, K., Kang, Y. S., Effect of amino acids in polymer/silver salt complex membranes on facilitated olefin transport. *J. Membrane Sci.*, **2004**, *248*, 201–206 (2004). DOI: 10.1016/j.memsci.2004.08.028

[17] Kim, J. H., Wong, J., Kang, Y. S., Olefin-induced dissolution of silver salts physically dispersed in inert polymers and their application to olefin/paraffin separation. *J. Membrane Sci.*, **2004**, *241*, 403–407. DOI: 10.1016/j.memsci.2004.05.027

[18] Lim, P. Y., Liu, R. S., She, P. L., Hung, C. F., Shih, H. C., Synthesis of Ag nanospheres particles in ethylene glycol by electrochemical-assisted polyol process, *Chem. Phys. Lett.*, **2006**, *420*, 304–308. DOI: 10.1016/j.cplett.2005.12.075

[19] Padmasree, K. P., Kanchan, D. K., Modulus studies ofCdI$_2$–Ag$_2$O–V$_2$O$_5$–B$_2$O$_3$ system. *Mater. Sci. Eng. B*, **2005**, *122*, 24–28 (2005). DOI: 10.1016/j.mseb.2005.04.011

[20] Ram, M., Chakrabarti, S., Dielectric and modulus studies on LiFe$_{1/2}$Co$_{1/2}$VO$_4$. *J. Alloys Compd.*, **2008**, *462*, 214–219. DOI: 10.1016/j.jallcom.2007.08.001

[21] Yahya M. Z. A., Arof, A. K., Conductivity and X-ray photoelectron studies on lithium acetate doped chitosan films. *Carbohydrate Polym.*, **2004**, *55*, 95–100. DOI: 10.1016/j.carbpol.2003.08.018

[22] Pradhan, D. K., Choudhary, R. N. P., Samantaray, B. K., Studies of the structural, thermal and electrical behavior of polymer nanocomposite electrolytes. *Express Polym. Lett.*, **2008**, *2*, 630–638. DOI: 10.3144/expresspolymlett.2008.76

[23] Yakuphanoglu, F., Electrical conductivity and electrical modulus properties of dihexylsexithiophene organic semiconductor. *Physica B*, **2007**, *393*, 139–142. DOI: 10.1016/j.physb.2006.12.075

[24] Dutta, A., Sinha, T. P., Jena, P., Adak, S., Ac conductivity and dielectric relaxation in ionically conducting soda-lime-silicate glasses. *J. Non-Cryst. Solids*, **2008**, *354*, 3952–3957. DOI: 10.1016/j.jnoncrysol.2008.05.028

[25] Patro, L. N., Hariharan, K., AC conductivity and scaling studies of polycrystalline SnF$_2$. *Mater. Chem. Phys.*, **2009**, *116*, 81–87. DOI: 10.1016/j.matchemphys.2009.0

[26] Patro, L. N., Hariharan, K.: Frequency-dependent conduction characteristics of mechanochemically synthesized NaSn$_2$F$_5$. *Mater. Sci. Eng., B*, **2009**, *162*, 173–178. DOI: 10.1016/j.mseb.2009.04.003

[27] Kwan, K. C., *Dielectric phenomena in solids*. Elsevier, New York, 2004.

[28] Calleja, R. D., Matveeva, E. S., Parkhutik, V. P., Electric relaxation in chemically synthesized polyaniline: Study using electric modulus formalism. *J. Non-Cryst. Solids*, **1995**, *180*, 260–265. DOI: 10.1016/0022-3093(94)00470-6

[29] Psarras, G. C., Gatos, K. G., Karahaliou, P. K., Georga, S. N., Krontiras, C. A., Karger-Kocsis, J., Relaxation phenomena in rubber/layered silicate nanocomposites. *Express Polym. Lett.*, **2007**, *1*, 837–845. DOI: 10.3144/expresspolymlett.2007.116

[30] Sengwa, R. J., Choudhary, S., Sankhla, S.: Low-frequency dielectric relaxation processes and ionic conductivity of montmorillonite clay nanoparticles colloidal suspension in poly(vinyl pyrrolidone)-ethylene glycol blends. *Express Polym. Lett.*, **2008**, *2*, 800–809. DOI: 10.3144/expresspolymlett.2008.93

[31] Lu, J., Suarez, J. J. B., Takahashi, A., Haruta, M., Oyama, S. T., In situ UV-vis studies of the effect of particle size on the epoxidation of ethylene and propylene on supported silver catalysts with molecular oxygen. *J. Catal.*, **2005**, *232*, 285–295 (2005). DOI: 10.1016/j.jcat.2005.02.013

[32] Kim, J. H., Kim, C. K., Won, J., Kang, Y. S., Role of anions for the reduction behavior of silver ions in polymer/silver salt complex membranes. *J. Membrane Sci.*, **2005**, *250*, 207–214 (2005). DOI: 10.1016/j.memsci.2004.10.032

[33] Liu, Y., Chen, S., Zhong, L., Wu, G., Preparation of high-stable silver nanoparticle dispersion by using sodium alginate as a stabilizer under gamma radiation. *Radiat. Phys. Chem.*, **2009**, *78*, 251–255. DOI: 10.1016/j.radphyschem.2009.01.003

[34] Kim, J. H., Min, B. R., Kim, H. S., Won, J., Kang, Y. S., Facilitated transport of ethylene across polymer membranes containing silver salt: Effect of HBF$_4$ on the photoreduction of silver ions. *J. Membrane Sci.*, **2003**, *212*, 283–288. DOI: 10.1016/S0376-7388(02)00451-9

[35] Sharma, V. K., Yngard, R. A., Lin, Y., Silver nanoparticles: Green synthesis and their antimicrobial activities. *Adv. Colloid Interface Sci.*, **2009**, *145*, 83–96. DOI: 10.1016/j.cis.2008.09.002

[36] Silvert, P-Y., Herrera-Urbina, R., Duvauchelle, N., Vijayakrishnan, V., Elhsissen, K. T., Preparation of colloidal silver dispersions by the polyol process. Part 1 – Synthesis and characterization. *J. Mater. Chem.*, **1997**, *7*, 293–299 (1997). DOI: 10.1039/JM9960600573

[37] Kang, S. W., Kim, J. H., Oh, K., Won, S. J., Char, K., Kim, H. S., Kang, Y. S. Highly stabilized silver polymer electrolytes and their application to facilitated olefin transport membranes. *J. Membrane Sci.*, **2004**, *236*, 163–169. DOI: 10.1016/j.memsci.2004.02.020

[38] Srivastava, S., Haridas, M., Basu, J. K., Optical properties of polymer nanocomposites. *Bull. Mater. Sci.*, **2008**, **31**, 213–217. DOI https://doi.org/10.1007/s12034-008-0038-9

[39] Zieli´nska, A., Skwarek, E., Zaleska, A., Gazda, M., Hupka, J., Preparation of silver nanoparticles with controlled particle size. *Procedia Chem.*, **2009**, *1*, 1560–1566. DOI: 10.1016/j.proche.2009.11.004

[40] Lin, H-W., Hwu, W-H., Ger, M-D., The dispersion of silver nanoparticles with physical dispersal procedures. *J. Mater. Process. Technol.*, **2008**, *206*, 56–61. DOI: 10.1016/j.jmatprotec.2007.12.025

Received: 19.05.2019
Accepted: 15.07.2019

EVALUATION OF ANTIOXIDANT ACTIVITY OF CINNAMIC ACID AND SOME OF ITS DERIVATIVES

Olawale H. Oladimeji,[a]* Aniekeme E. Essien,[a] Arthur J. Sheriff[a] and Taiwo E. Alemika[b]

Keywords: Cinnamic acid; esterification; selective-reduction; ethyl cinnamate; cinnamyl alcohol.

Cinnamic acid, chemically known as 3-phenyl-2-propenoic acid is has a broad spectrum of pharmacological actions including antioxidant activity. The esterification and selective reduction of the acid led to ethyl cinnamate and cinnamyl alcohol, respectively. Cinnamic acid demonstrated a poor antioxidant activity (IC_{50}) of 1.2 μg mL^{-1} while ethyl cinnamate and cinnamyl alcohol elicited activities of 0.64 μg mL^{-1} (moderate) and 0.84 μg mL^{-1}, respectively. The obtained results indicate that esterification enhances the antioxidant activity of cinnamic acid.

* Corresponding Authors
E-Mail: wale430@yahoo.co.uk; hakeemoladmeji@uniuyo.edu.ng
[a] Department of Pharmaceutical and Medicinal Chemistry, Faculty of Pharmacy, University of Uyo, Uyo, Nigeria.
[b] Department of Pharmaceutical Chemistry, Faculty of Pharmaceutical Sciences, University of Jos, Nigeria

INTRODUCTION

Free-radicals are chemical species which have been implicated as the causative agents in many degenerative conditions such as Alzheimer's and Parkinson's disease, stroke, cancer, pancreatitis, laryngitis, asthma, hay fever, rheumatoid arthritis, wounds, atherosclerosis, emphysema, lungs dysfunction, radiation injuries, premature aging and diabetes amongst many others.[1-4] Living organism possesses antioxidant defense and repair system which offer some protections against oxidative stress but nevertheless are insufficient to prevent the damage. Antioxidants are believed to play an important role in the body defence system against radical oxidative species (ROS)[5-6] and at low concentrations significantly delay or inhibit oxidation of body tissues.[7]

Some of the antioxidant drugs in clinical practice are costly, toxic and poorly active. Hence, there is need to search for templates with little or no toxicities. A known chemical substance with antioxidant activity, cinnamic acid was considered. It is a white colored crystalline organic acid occurring naturally in plants which has low toxicity and a broad spectrum of biological activities. This acid is used as a flavoring agent in certain pharmaceuticals and in the manufacture of the esters for the perfume and fragrance industry. Cinnamic acid can being structurally modified into compounds with probable potentials for higher antioxidant activities. In the present study, the acid was chemically modified to its ethyl ester and reduced derivatives by esterification and $NaBH_4$-reduction (selective reduction) respectively. The acid and synthesized products were screened for antioxidant activities using the DPPH (2,2-diphenyl-1-picrylhydrazyl hydrate) reagent and the obtained antioxidant activities (IC_{50}) compared.

EXPERIMENTALS

Cinnamic acid and DPPH (2, 2-diphenyl-1-picrylhydrazyl hydrate**)** were sourced from Sigma Chemicals, Germany) while acetic acid, acetone, benzene, chloroform, diethyl ether, ethanol, hydrochloric acid, magnesium sulphate, methanol, petroleum ether, sodium borohydride, sodium hydroxide, sulphuric acid and tetrahydrofuran were obtained as AnaLAR Grade Chemicals from BDH Chemicals Limited Poole, England.

Melting points were determined using an Electro-thermal Melting Point apparatus (Electro-thermal Engineering Limited, England).[8] The properties of the cinnamic acid and derivatives are the followings:

Cinnamic acid: $C_9H_8O_2$; mol. wt. (148.16 g/mol); white color crystalline solid; m.pt. (132-134 ^0C); $[n]_D^{20}$ (1.616); $[\alpha]_D^{20}$ (0^0); [d] (1.25 g /cm^3): FTIR (cm^{-1}): 1576 (Ar-C=C), 1627 (acyclic C=C), 1682 (α, β unsaturated C=O), and 2923 (-OH).

Ethyl cinnamate: $C_{11}H_{12}O_2$; mol. wt. (176.21 g/mol); pale-yellow liquid; $[n]_D^{20}$ (1.658); $[\alpha]_D^{20}$ (0^0); [d] (1.05 g /cm^3): FTIR (cm^{-1}): 711, 767 (CH_2 and CH_3 bending modes), 1037 (C-O-C, ether linkage), 1637 (Ar-C=C) and 1730 (C=O).

Cinnamyl alcohol: $C_9H_{10}O_1$; mol. wt. (134.16 g/mol); colorless liquid; $[n]_D^{20}$ (1.581); $[\alpha]_D^{20}$ (0^0); [d] (1.04 g /cm^3): FTIR (cm^{-1}): 754, 1631 (Ar-C=C), 1681 (acyclic C=C) and 3200 (-OH).

Assays

Cinnamic acid (1.5 g) was carefully weighed out into a conical flask and 50 mL of 0.5 M NaOH added. The mixture was immersed in boiling water bath for 10 minutes, cooled and three drops of phenolphthalein were added as indicator. Titration was then carried out against the excess alkali using 0.5 M HCl and the end-point noted (pink color). Blank titration was carried out without the sample.

Ethyl cinnamate synthesis[9]

Cinnamic acid (1.0 g) was dissolved in 100 mL of ethanol and 10 mL of cc, sulphuric acid was added. The flask was corked with Al foil and kept for 2 weeks in a refrigerator at 4 ^{0}C to ensure complete synthesis of the ester.

Selective reduction of cinnamic acid[10]

Cinnamic acid (1.5 g) was dissolved in 20 mL of THF and this solution was slowly added to a suspension of $NaBH_4$ (0.45 g) in 200 mL of THF at room temperature in 10 min. The mixture was stirred until evolution of gas ceased. 0.63 g of iodine and 20 mL of THF were carefully added to the mixture immersed in an ice-bath with the evolution of more gas. The mixture was further stirred for 1 h. Dilute HCl (5 mL) was added carefully and the mixture extracted with ether. The combined ethereal extracts was washed with 3 M NaOH (30 mL), brine and dried over $MgSO_4$. Evaporation of the organic layer gave the reduced product.

Determination of optical rotation and refractive index

Cinnamic acid was dissolved methanol and the optical rotation was measured at 589.3 nm at 20.5 ^{0}C with using an ADP-220 (Bellingham Stanley, England) polarimeter. The refractive indexes were measured on a WAY-15 (Abbe, England) refractometer at the same wavelength and temperature.[11-12] The optical rotation and refractive indices of the derivatives being liquids were measured directly without dissolution in any solvents.

Spectrophotometric determination of antioxidant activity using DPPH reagent

Substances which are capable of donating electrons or hydrogen atoms can convert the purple-colored DPPH radical (2,2-diphenyl-1-picrylhydrazyl hydrate) to its yellow-colored non-radical form; 1,1-diphenyl-2-picrylhydrazine.[13-14] The absorbance of each sample was taken at λ_m 512 nm using a Jenway 6405 (USA) UV-spectrophotometer.

Determination of the antioxidant activity of cinnamic acid, its derivatives and vitamin C

Each of sample (2 mg) was dissolved in 50 mL of methanol. Serial dilutions were carried out and each concentration was incubated with same volume of 0.004 % w/v methanolic DPPH solution for optimal analytical accuracy. After an incubation period of 30 minutes in the dark at room temperature (25 ± 2 ^{0}C), the absorbance of each test sample was then taken at λ_m 512 nm. The radical scavenging activity (RSA %) or percentage inhibition (PI %) of free radical DPPH were calculated according to th stahdard equation:

$$RSA(PI,\%) = 100\,\frac{A_{\text{blank}} - A_{\text{sample}}}{A_{\text{blank}}}$$

where A_{blank} is the absorbance of the control reaction (DPPH solution without the test sample and A_{sample} is the absorbance of DPPH incubated with the samples. Vitamin C concentration providing 50 % inhibition (IC_{50}) was calculated from a graph of inhibition percentage against the concentration of the samples and Vitamin C.[15-16]

Infrared spectroscopy

IR spectra were recorded with a Shimadzu 8400S FT-IR (Japan) spectrophotometer.

RESULTS AND DISCUSSION

Cinnamic acid used in this study was subjected to analysis for ascertaining and establishing its purity. Its melting point was found to be 132-134 ^{0}C. The percentage purity of the sample of cinnamic acid was computed to be 97.27 % w/w from the back-titration of sodium hydroxide. Its refractive index was found to be 1.616 and there was no optical rotation. Diagnostic IR stretchings at 1576, 1627, 1682 and 2923 cm^{-1} indicate the characteristic Ar-C=C, acyclic C=C, α, β unsaturated C=O and –OH groups, respectively.

Ethyl cinnamate was synthesized as a pale yellow liquid. This compound was isolated as a yellow oil from *Pycnanthus angolensis* (Welw.) Warb using column chromatography (CC) and preparative column chromatography (p TLC) and characterized by IR and GC/MS techniques.[17] Its refractive index was found to be 1.658.

Cinnamyl alcohol was synthesized by the selective-reduction method.[10] This procedure converts a carboxylic acid to an alcohol using sodium borohydride in the presence of iodine. Its refractive index was found to be 1.581.

Table 1. Radical scavenging activity (percentage inhibition) of samples at different concentrations and IC_{50} values of samples

Sample	**Concentration, mg mL^{-1}**					**IC_{50}, µg mL^{-1}**
	0.0004	**0.0008**	**0.0012**	**0.0016**	**0.0020**	
Cinnamic acid	43.28	46.78	50.98	57.98	62.18	1.2
Ethyl cinnamate	46.50	52.38	58.54	64.42	71.84	0.64
Cinnamyl alcohol	41.10	50.98	55.18	63.58	69.18	0.84
Vitamin C	87.10	87.39	87.69	88.09	88.70	0.34

Antioxidant activity

The radical scavenging activity (RSA %) or percentage inhibition (PI %) and the IC$_{50}$ values of the studied cinnamic acid derivatives or Vitamin C are given in Table 1. Ethyl cinnamate gave a moderate antioxidant activity (IC$_{50}$) of 0.64 μg mL^{-1} while the activity of reduced derivative was marginal at 0.84 μg mL^{-1} Cinnamic acid was poorly active (1.2 μg mL^{-1}).

Ethyl cinnamate demonstrated a higher antioxidant activity than cinnamic acid due to its lipophilic character. Hence, ethyl cinnamate is able to transverse the lipid membrane to the allosteric (active) sites better and faster than cinnamic acid to effect the pharmacological action of anti-oxidation. Ethyl cinnamate isolated from *P. angolensis* (Welw.) Warb was found to be antioxidant at 0.48 μg mL^{-1} [18-20] while the synthesized one showed an activity of 0.64 μg mL^{-1}.

CONCLUSION

The results of this present study indicate that the esterification of cinnamic acid enhances its antioxidant activity which compare favorably with the activity elicited by a standard antioxidant drug (Vitamin C).

ACKNOWLEDGEMENTS

The authors gladly acknowledge the kind gesture of the Department of Pharmaceutical and Medicinal Chemistry, University of Uyo for the use of its Jenway 6405 UV/VIS spectrophotometer in the antioxidant assays. Also, we are grateful to the University of Ibadan, Nigeria for use of their Infra-Red Spectrophotometer (FTIR, Shimadzu, Japan) in the IR analyses.

REFERENCES

[1] Toda, S., Shirataki, Y., Inhibitory effects of isoflavones in roots of *Astralagus membranaceus* (Astralagus radix) on lipid peroxidation by reactive oxygen species. *Phytother. Res.*, **1998**, *12(1)*, 59-61. https://DOI.org/10.1002/(SICI)1099.1573(19980201)12:1‹59:AID-PTR182›3.0.CO;2-R

[2] Speroni, E., Guerra, M. C., Minghetti, A., Cerspi-Perellino, N., Pusini, P., Roda, A., Oleuropein evaluated *in-vitro* and *in-vivo* as an antioxidant. *Phytother. Res.*, **1998**, *12*, 98-100. https://DOI:10.1002(SICI)1098-1573(1998)12:1+‹S98:AID-PTR263›3.0.CO;2-M.

[3] Guyton, M., Hall, B., *Textbook on medical physiology*, 11th ed., Elsevier Publishers, **2006**, pp. 65-72.

[4] Piper, T., *Stedman's medical dictionary*. Lippincott Williams and Wilkins, **2006**, pp. 56-57.

[5] Ou, B., Huang, D., Hampsch-Woodill, M., Flanagan, J. A., Deemer, E. K., Analysis of antioxidant activities of common vegetables employing oxygen radical absorbance capacity and ferric reducing antioxidant power assay. A comparative study. *J. Agric. Food Chain.*, **2002**, *5*, 233-228. DOI:10.1021/jf01/235c/boxin.

[6] Vivek, K. G., Surendra, K. S., Plants as natural antioxidants. *Nat. Prod. Rad.*, **2006**, *5(4)*, 326-334. DOI:10:1016/0378-8741(87)90125-5.

[7] Halliwell, B., Gutteridge, J. M. C., The definition and measurement of antioxidants in biological systems. *Free Rad. Biol. and Med.*, **1995**, *18*, 125-126. DOI :10.106/0801-5849(95)91457-3.

[8] B. P., *British Pharmacopeia, The Pharmaceutical Press London, Appendix VA, A109*, 1993, p. 754.

[9] Morrison, R. T, Boyd, R. N., *Organic chemistry*. *Allyn and Bacon Inc.*, 1973, pp. 602-603 and 672-673.

[10] Bhaskar-Kanth, J.V, Periasamy, M., Selective reduction of carboxylic acids into alcohols using NaBH$_4$ and I$_2$. *J. Org. Chem.*, **1991**, *56(20)*, 5964-5965. DOI:10.1021/jo00020a052.

[11] Olaniyi, A., Ogungbamila, F. O., *Experimental pharmaceutical chemistry*. Shaneson C. I. Limited, **1991**, pp. 49-52.

[12] Olaniyi, A. A., *Principles of quality assurance and pharmaceutical analysis*. Mosuro publishers, **2000**, pp. 151-158, 216-217, 264-269 and 443-457.

[13] Nagalapur, S. K., Paramjyothi, S., *In-vitro* antioxidant activity of *Launaea pinnatifida* Cass leaves. *The Bioscan*, **2010**, *5(1)*, 105-108. www.thebioscan.in/journals/abs2010.5nl_105_108htm.

[14] Guangrong, H., Jiaxin, J., Dehui, D., Anti-oxidative and antibacterial activity of the methanol extract of *Artemisia anomala* S. Moore. *Afric. J. Biotech.*, **2008**, 7(9), 1335-1338. DOI:10.1011060.8245

[15] Lebeau, J., Furman, G., Bernier, J. L., Durietz, P., Teissier, E., Cotelle, N., Antioxidant properties of di-tert-butylhydroxylated flavonoids. *Free-Radical Biology and Med.*, **2000**, *29(9)*, 900-912. https://doi.org/10.1016/s0891-5849 (00)00390-7.

[16] Leitao, G. G., Leitao, S. G., Vilegas, W., Z. Quick preparative separation of natural naphthoquinones with antioxidant activity by high speed counter current chromatography, Z. *Naturforsch*, **2002**, *57C*, 1051-1055. https://doi.org/10.1515/znc-2002-11-1217.

[17] Oladimeji, H. O., Onu, O. N., Isolation of ethyl cinnamate and substituted fluorene from *Pycnanthus angolensis* (Welw) Warb. *Eur. Chem. Bull.*, **2017**, *6(9)*, 421-423, DOI: 10.17628/ecb.2017.6.421-423.

[18] Oladimeji, H. O, Ahmadu, A. A., Antioxidant activity of compounds isolated from *Pycnanthus angolensis* (Welw.) Warb and *Byrophyllum pinnatum* (Lam) Oken. *Eur. Chem. Bull.*, **2019**, *8(3)*, 96-100. DOI: 10.17628/ecb.2019.8.96-100.

[19] Bunta, G. W., Ingold, R. U., β-carotene: An unusual type of lipid antioxidant. *Science*, **1984,** *224*, 569-573. https://doi.org/10.1126/ science.6710156.

[20] Dapkevicius, A., Vanskulons, R., Van-Beek, T. A., Linssen, J. P., Antioxidant activity of extracts obtained by different isolation procedures from some aromatic herbs grown in *Lithuania. J. Sci. Food Agric.*, **1998**, *77(1)*, 140-146. https://doi.org/10.1002/(sici)1097-0010(199805)77:1<140::aid-jsfa18>3.3.co;2-b

Received: 18.05.2019.
Accepted: 15.07.2019.

A CONVENIENT CATALYST-FREE SYNTHESIS OF SOME SUBSTITUTED PYRIDINE BENZAMIDES FROM ARYL ALDEHYDES

Vaishanavi S. Jambhorkar,[a] Aniket P. Sarkate,[a]* Aishwarya P. Rajhans,[a] Kshipra S. Karnik,[a] Sajed H. Ansari,[a] Shambala U. Chavan,[a] Yogesh W. More,[b] Dattatraya N. Pansare[b]

Keywords: benzamides; aldehydes; aminopyridines; hydrogen peroxide; catalyst-free.

A new method of amides synthesis under catalyst-free condition has been developed by using aldehydes and aminopyridines. The amides were synthesized by using different aldehydes and aminopyridines using ethanol as a solvent and hydrogen peroxide as oxidant. The method helps in preparation of amides which were acquired in good yield within 4-5 h using conventional heating. The reaction is catalyst-free. The developed method is easy, economical, and flexible.

*Corresponding Authors
E-Mail: dbsaniket09@gmail.com
[a] Department of Chemical Technology, Dr. Babasaheb Ambedkar Marathwada University, Aurangabad, 431004 (MS), India
[b] Department of Chemistry, Deogiri College, Station road, Aurangabad- 431005 (MS), India

INTRODUCTION

The amide bond is one of the most important functional group. Amides are the precursors of polymers, proteins and many natural compounds.[1] The preparation of peptides involves amide bond formation.[2] The synthesis of amides is generally done by the reaction of amines with active derivatives of carboxylic acid such as anhydrides, acyl halides, aldehydes, and esters.[3] Benzamides having biological significance and potency as effective antihelmintic or antimicrobial agents and proved to be a potent smooth muscle relaxant. Synthesis of these benzamides includes many methods such as the direct conversion of benzene, electrophilic aromatic substitution reaction, etc.[5]

Due to their potential importance in pharmaceutical fields, catalyst-free reactions are the most emerging concept in the last few decades in the organic synthesis.[6,7] A catalyst-free reaction has of extreme significance in decreasing the amount of by-products which avoids purification of compounds.[8] Hydrogen peroxide has high active oxygen content and water as a reduced product which can be easily removed.[9] Ethanol produced from renewable biomass[10] and used as a solvent because of its chemical and toxicological limitation.[11] As it is readily soluble in water thus, it avoids obstruction during workup procedure.[12]

In continuation of our previous work[13-26] for the synthesis of pharmaceutically active materials, an alternative pathway is given for synthesis of pyridine benzamides.

EXPERIMENTAL

All chemicals, unless otherwise specified, were purchased from commercial sources and were used without further purification. The major chemicals were purchased from Sigma Aldrich and Avra labs. The development of reactions was monitored by thin-layer chromatography (TLC) analysis on Merck pre-coated silica gel 60 F254 aluminum sheets, visualized by UV light. Melting points were recorded on SRS Optimelt. Melting points are uncorrected. The ^{1}H NMR spectra were recorded on a 400 MHz Varian NMR spectrometer, shifts are reported in δ_{ppm} units. The ^{13}C were recorded on a 100 MHz Varian NMR spectrometer.

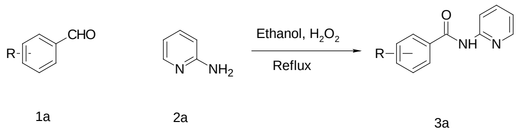

Scheme 1.

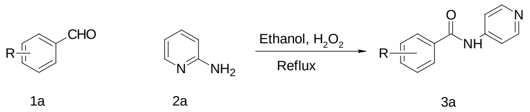

Scheme 2.

General procedure for the synthesis of benzamide compounds

To the mixture of aldehyde (0.1 g, 0.00094 mol) and aminopyridine (1 eq.), ethanol (5-7 mL) was added as a solvent and stirred for 15 min. After the dissolution of reactant, the reaction mixture was refluxed was 4-5 h with the addition of H_2O_2. After the completion of the reaction, the product was extracted with ethyl acetate and water. The solvent was evaporated to dryness to afford the product.

DOI: http://dx.doi.org/10.17628/ecb.2019.8.227-230

N-(Pyridin-2-yl)benzamide (3a)

^{1}H NMR (400 MHz, DMSO-d_6) 8.41 (d, 1H), 8.15 (d, 1H), 7.99 (d, 2H), 7.80 (t, 1H), 7.49 (d, 2H), 7.15(t, 1H). ^{13}C NMR 165.4, 151.0, 149.2, 137.1, 132.4, 129.3, 129.1, 119.2, 114.8.

4-Chloro-N-(pyridin-2-yl)benzamide (3b)

^{1}H NMR (400 MHz, DMSO-d_6) 8.15(d, 1H), 8.14(d, 1H), 7.95 (d, 2H), 7.80 (t, 1H), 7.55 (t, 1H), 7.48 (t, 2H), 7.17 (t, 1H).^{13}C NMR 165.6, 151.4, 149.2, 138.4, 133.9, 132.4, 128.5, 128.2, 119.2, 114.5.

2-Chloro-N-(pyridin-2-yl)benzamide (3c)

^{1}H NMR (400 MHz, DMSO-d_6) 8.41 (d, 1H), 8.14 (d, 1H), 7.82 (d, 2H), 7.43 (d, 1H), 7.41 (d, 1H), 7.40 (d, 1H), 7.16 (t, 1H). ^{13}C NMR 164.7, 150.8, 149.1, 138.3, 132.2, 131.6, 131.4, 129.9, 129.6, 126.5, 119.2, 115.1.

4-Bromo-N-(pyridin-2-yl)benzamide (3d)

^{1}H NMR (400 MHz, DMSO-d_6) 8.14 (d, 1H), 8.16 (d, 1H), 7.92 (d, 2H), 7.89 (t, 1H), 7.64 (d, 2H), 7.15 (t, 1H). ^{13}C NMR 165.8, 151.0, 149.2, 138.0, 132.7, 131.8, 129.2, 124.3, 119.2, 114.8.

2-Nitro-N-(pyridin-2-yl)benzamide (3e)

^{1}H NMR (400 MHz, DMSO-d_6) 8.41 (d, 1H), 8.26 (d, 1H), 8.03(d, 1H), 7.80 (t, 1H), 7.79 (t, 1H), 7.77 (t, 1H), 7.14 (t, 1H). ^{13}C NMR 164.9, 150.8, 149.2, 147.0, 138.0, 132.4, 131.1, 130.2, 129.5, 124.1, 119.2, 115.1.

4-Methoxy-N-(pyridin-2-yl)benzamide (3f)

^{1}H NMR (400 MHz, DMSO-d_6) 8.41 (d, 1H), 8.15 (d, 1H), 7.87 (d, 2H), 7.81 (t, 1H), 7.15 (t, 1H), 7.02 (d, 2H), 3.81(s, 3H). ^{13}C NMR 165.5, 161.9, 151.0, 149.1, 137.9, 130.1, 128.5, 119.2, 114.8, 113.5, 55.3.

4-Nitro-N-(pyridin-2-yl)benzamide (3g)

^{1}H NMR (400 MHz, DMSO-d_6) 8.40 (d, 1H), 8.33 (d, 2H), 8.12(d, 2H), 7.79 (t, 1H), 7.16 (t, 1H). ^{13}C NMR 166.2, 151.0, 149.4, 149.2, 137.9, 136.3, 128.9, 124.1, 119.2, 114.8.

2,3-Dimethyl-N-(pyridin-2-yl)benzamide (3h)

^{1}H NMR 8.40 (d, 1H), 8.15(d, 1H), 7.80 (t, 1H), 7.65 (d, 1H), 7.15(m, 3H), 2.39 (s, 3H), 2.30 (s, 3H). ^{13}C NMR 165.9, 150.8, 149.1, 138.2, 137.3, 134.4, 134.2, 132.0, 136.2, 125.6, 119.2, 115.1, 20.0, 16.5.

3,4-Dimethoxy-N-(pyridin-2-yl)benzamide (3i)

^{1}H NMR (400 MHz, DMSO-d_6) 8.40 (d, 1H), 8.17(d, 1H), 7.80 (t, 1H), 7.45 (t, 2H), 7.15(t, 1H), 6.98 (d, 3H), 3.87 (s, 3H), 3.91 (s, 3H). ^{13}C NMR 166.0, 152.3, 150.8, 149.2, 149.2, 137.9, 129.2, 122.6, 119.2, 114.6, 111.5, 111.4, 55.9, 55.9.

N-(Pyridin-4-yl)benzamide (5a)

^{1}H NMR (400 MHz, DMSO-d_6) 9.50 (s, 1H), 8.40 (d, 2H), 7.96 (t, 4H), 7.50 (t, 2H), 7.46 (d, 1H). ^{13}C NMR 168.3, 148.9, 143.2, 134.5, 132.4, 128.6, 127.7, 113.7.

2-Chloro-N-(pyridin-4-yl)benzamide (5b)

^{1}H NMR (400 MHz, DMSO-d_6) 9.18(s, 1H), 8.40(d, 2H), 7.99(d, 1H), 7.98(d, 1H), 7.75(t, 1H), 7.47(d, 1H), 7.41(t, 1H), 7.40(d, 1H). ^{13}C NMR 165.1, 148.9, 143.3, 132.2, 131.8, 131.4, 129.9, 126.6, 126.5, 113.4.

2-Nitro-N-(pyridin-4-yl)benzamide (5c)

^{1}H NMR (400 MHz, DMSO-d_6) 9.88 (s, 1H), 8.40 (d, 1H), 8.19 (d, 1H), 8.04 (d, 1H), 7.95 (d, 2H), 7.82 (t, 1H), 7.74(t, 1H). ^{13}C NMR 165.3, 148.9, 147.0, 143.3, 132.4, 131.1, 130.5, 129.7, 123.6, 113.5.

4-Bromo-N-(pyridin-4-yl)benzamide (5d)

^{1}H NMR (400 MHz, DMSO-d_6) 9.88 (s, 1H), 8.40 (d, 2H), 7.93 (d, 2H), 7.86 (d, 2H), 7.65 (d, 2H). ^{13}C NMR 169.6, 149.1, 143.3, 133.7, 131.8, 129.3, 124.3, 113.8.

4-Methoxy-N-(pyridin-4-yl)benzamide (5e)

^{1}H NMR (400 MHz, DMSO-d_6) 8.40 (d, 1H), 7.98 (d, 1H), 7.87 (d, 1H), 7.03 (d, 1H), 3.81 (s, 2H). ^{13}C NMR 169.9, 161.9, 148.9, 143.3, 129.7, 129.1, 113.8, 113.5, 55.3.

RESULTS AND DISCUSSION

The reaction to prepare compound **3a** was screened with different solvents to enhance the competence of the reactants and the results are as summarized in Table 1.

Table 1. Optimization of solvents in the preparation of **3a**

Solvent	Time, h	Yield, %
N,N-Dimethylformamide	29	87
Toluene	12	65
Water	10	75
Ethanol	5	99

It could be observed that other than reported[1] the use of ethanol as a solvent proves beneficial in the percentage yield and reaction time as well. On the reaction with N,N-dimethylformamide, the yield was up to the mark, but the reaction time made us look forward towards other solvents (Table 1). On the other hand, the use of toluene showed a drastic change in the reaction time, but the purification reduced the yield of the compound.

Water gave less percentage yield than expected, but the reaction time reduced to 10 h. Ethanol paved us the way towards a further synthesis because of reduced reaction time and excellent yield.

Table 2. Preparation of 2-substituted pyridine benzamide compounds **(3a-m)** in the presence of H_2O_2 in EtOH

Sr. No	$R^1R^2C_6H_3CHO$	Benzamide product	
		Time, h	Yield, %
3a	R^1=H, R^2=H	4	99
3b	R^1=4-Cl, R^2=H	4	94
3c	R^1=2-Cl, R^2=H	5	95
3d	R^1=4-Br, R^2=H	4	85
3e	R^1=2-NO_2, R^2=H	5	80
3f	R^1=4-MeO, R^2=H	5	95
3g	R^1=4-NO_2, R^2=H	5	90
3h	R^1=R^2=Me	4	87
3i	R^1=R^2=MeO	5	92

In preparation of 4-substituted pyridine benzamide (**5a**) (Scheme 2), the optimization of different solvents (Table 2) gave us similar results as were established in case of 2-substituted pyridine derivative (**3a**). The yield and the time required for the reactions were quite similar to those of compound **3a**.

Table 3. Optimization of solvents in the preparation of **5a.**

Solvent	Time, h	Yield, %
N,N-Dimethylformamide	29	84
Toluene	12	55
Water	10	80
Ethanol	5	95

Table 4. Preparation of 4-substituted pyridine benzamide compounds **(5a-e)** in the presence of H_2O_2 in EtOH

Sr. No	$R^1R^2C_6H_3CHO$	Benzamide product	
		Time, h	Yield, %
5a	R^1=H, R^2=H	5	88
5b	R^1=2-Cl, R^2=H	4	95
5c	R^1=2-NO_2, R^2=H	4	83
5d	R^1=4-Br, R^2=H	5	80
5e	R^1=4-MeO, R^2=H	4	92

CONCLUSION

We have optimized a catalyst-free one-pot synthesis of benzamide from substituted aldehyde and aminopyridines with excellent yields. The solvent as ethanol and oxidant as H_2O_2 plays an important role to give promising yields. As the reaction is catalyst-free, thus this reaction proves to be economical and advantageous.

Acknowledgment

The authors are thankful to The Head, Department of Chemical Technology, Dr. Babasaheb Ambedkar Marathwada University, Aurangabad 431 004 (MS), India, for providing the laboratory facility.

REFERENCES

[1] Yang, S., Yan, H., Xiao, Yu. R, Xiao, Yu, S., Li, J., Wang, Y., Copper-catalyzed dehydrogenative reaction: synthesis of amide from aldehydes and aminopyridine, *Tetrahedron*, **2013**, *69*, 6431. https://doi.org/10.1016/j.tet.2013.05.072

[2] Joullie, M. M., Lassen, M. K., Evolution of amide bond formation, *Arkivoc*, **2010**, *(viii)*, 189.

http://dx.doi.org/10.3998/ark.5550190.0011.816

[3] Feng, J. B., Wei, D., Gong, J. L., Qi, X., Wu, X. F., Oxidative synthesis of benzamides from toluenes and DMF, *Tetrahedron Lett*., **2014**, *55*, 5082.

https://doi.org/10.1016/j.tetlet.2014.07.083

[4] Kumar, A., Narasimhan, B., Kumar, D., Synthesis, antimicrobial, and QSAR studies of substituted benzamides, *Bioorg. Med. Chem.*, **2007**, *15*, 4113.

https://doi.org/10.1016/j.bmc.2007.03.074

[5] Peng, H., Xu, L., Wu, H., Zhang, K., Wu, P., One-pot synthesis of benzamide over a robust tandem catalyst based on center radially fibrous silica encapsulated TS-1, *Chem Comm*., **2013**, *49*, 2709. https://doi.org/10.1039/C3CC38546A

[6] Gawande, M., Bonifacio, V., Luque, R., Branco, P., Varma, R., Benign by design: catalyst-free in-water, on-water green chemical methodologies in organic synthesis, *Chem. Soc. Rev*., **2013**, *42*, 5522. https://doi.org/10.1039/C3CS60025D

[7] Mashkouri, S., Naimi-Jamal, M. R., Mechanochemical solvent-free and catalyst-free one-pot synthesis of pyrano[2,3-*d*]Pyrimidine-2,4(1H,3H)-diones with Quantitative Yields, *Molecule*, **2009**, *14 (1)*, 474.

https://dx.doi.org/10.3390%2Fmolecules14010474

[8] Hasaninejad, A., Zare, A., Shekouhy, M., Rad, J. A., Catalyst-Free One-Pot Four Component Synthesis of Polysubstituted Imidazoles in Neutral Ionic Liquid 1-Butyl-3-methylimidazolium Bromide, *J. Combinat. Chem*., **2010**, *12(6)*, 844. https://doi.org/10.1021/cc100097m

[9] Shu, L., Shi, Y., Asymmetric epoxidation using hydrogen peroxide (H_2O_2) as primary oxidant, *Tetrahedron Lett*., **1999**, *40*, 8721. https://doi.org/10.1016/S0040-4039(99)01814-6

[10] Matsumura, M., Maek, H., Application of solvent extraction to ethanol fermentation, *Appl. Micro. Biotech*., **1984**, *20*, 371. https://doi.org/10.1007/BF00261937

[11] Santamarıa, R. I., Reyes-Duarte, M. D., Barzana, E., Fernando, D., Gama, F. M., Mota, M., Lopez Munguıa, A., Selective Enzyme-Mediated Extraction of Capsaicinoids and Carotenoids from Chili Guajillo Puya (*Capsicum annuum* L.) Using Ethanol as Solvent, *J. Agric. Food. Chem*., **2000**, *48*, 3063. https://doi.org/10.1021/jf991242p

[12] Petong, P., Pottel, R., Kaatze, U., Water−Ethanol Mixtures at Different Compositions and Temperatures. A Dielectric Relaxation Study, *J. Phys. Chem. A.*, 2000, *104*, 7420. https://doi.org/10.1021/jp001393r

[13] Dofe, V. S., Sarkate, A. P., Shaikh, Z. M., Jadhav, C. K., Nipte, A. S., Gill, C. H., Ultrasound-assisted synthesis of novel pyrazole and pyrimidine derivatives as antimicrobial agents, *J. Heterocycl. Chem.*, **2018**, *55*, 756. https://doi.org/10.1002/jhet.3105

[14] Tiwari, S. V., Seijas, J. A., Vazquez-Tato, M. P., Sarkate, A. P., Karnik, K. S., Nikalje, A. P. G., Ionic Liquid Promoted Synthesis Of Novel Chromone-Pyrimidine Coupled Derivatives, Antimicrobial Analysis, Enzyme Assay, Docking Study And Toxicity Study, *Molecules*, **2018**, *23*, 1. https://doi.org/10.3390/molecules23020440

[15] Nikalje, A. P. G., Tiwari, S. V., Sarkate, A. P., Karnik, K. S., Imidazole-thiazole coupled derivatives as novel lanosterol 14-α demethylase inhibitors: Ionic liquid mediated synthesis, biological evaluation and molecular docking study, *Med. Chem. Res.*, **2018**, *27*, 592. https://doi.org/10.1007/s00044-017-2085-5

[16] Tiwari, S. V., Seijas, J. A., Vazquez-Tato, M. P., Sarkate, A. P., Karnik, K. S., Nikalje, A. P. G., Facile Synthesis Of Novel Coumarin Derivatives, Antimicrobial analysis, Enzyme Assay, Docking Study, ADMET Prediction And Toxicity Study, *Molecules*, **2017**, *22*, 1. https://doi.org/10.3390/molecules22071172

[17] Sarkate, A. P., Lokwani, D. K., Patil, A. A., Bhandari, S. V., Bothara, K. G., Synthesis and Evaluation of Anti-inflammatory, Analgesic, Ulcerogenicity and Nitric Oxide Releasing Studies of Novel Ibuprofen Analogs as Nonulcerogenic Derivatives, *Med. Chem. Res.*, **2011**, *20*, 795. https://doi.org/10.1007/s00044-010-9389-z

[18] Lokwani, D., Azad, R., Sarkate, A., Reddanna, P., Shinde, D., Structure-Based Library Design (SBLD) for New 1,4-dihydropyrimidine Scaffold as simultaneous COX-1/COX-2 and 5-LOX Inhibitors, *Bioorg. Med. Chem.*, **2015**, *23(15)*, 4533. https://doi.org/10.1016/j.bmc.2015.06.008

[19] Tiwari, S. V., Siddiqui, S., Seijas, J. A., Vazquez-Tato, M. P., Sarkate, A. P., Lokwani, D. K., Nikalje, A. P. G., Microwave-assisted Facile Synthesis, Anticancer Evaluation and Docking study Of *N*-((5-(substituted methylene amino)-1,3,4-thiadiazol-2-yl)methyl) Benzamide Derivatives, *Molecules*, **2017**, *22 (6)*, 995. https://doi.org/10.3390/molecules22060995

[20] Tiwari, S. V., Seijas, J. A., Vazquez-Tato, M. P., Sarkate, A. P., Lokwani, D. K., Nikalje, A. P. G., Ultrasound Mediated One-Pot, Three-Component Synthesis, Docking and ADME prediction of Novel 5-amino-2-(4-chlorophenyl)-7-substituted phenyl-8,8a-dihydro-7H-[1,3,4]thiadiazolo[3,2-α]pyrimidine-6-carbonitrile Derivatives as Anticancer Agents *Molecules* **2016**, *21 (8)*, 894. https://doi.org/10.3390/molecules21080894

[21] Pawar, C. D., Sarkate, A. P., Karnik, K. S., Bahekar, S. S., Pansare, D. N., Shelke R. N., Jawale, C. S., Shinde, D. B., Synthesis and antimicrobial evaluation of novel ethyl 2-(2-(4-substituted) acetamido)-4-substituted-thiazole-5-carboxylate derivatives, *Bioorg. Med. Chem. Lett.*, **2016**, *26 (15)*, 3525. https://doi.org/10.1016/j.bmcl.2016.06.030

[22] Dofe, V. S., Sarkate, A. P., Lokwani, D. K., Kathwate, S. H., Gill, C. H., Synthesis, antimicrobial evaluation, and molecular docking studies of novel chromone based 1,2,3-triazoles, *Res. Chem. Int.*, **2017**, *43 (1)*, 15. https://doi.org/10.1007/s11164-016-2602-z

[23] Sarkate, A. P., Bahekar, S. S., Wadhai, V. M., Ghandge, G. N., Wakte, P. S., Shinde, D. B., Microwave-assisted synthesis of non-symmetrical aryl ethers by using nitroarenes, *Synlett* **2013**, *24*, 1513. DOI: 10.1055/s-0033-1338869

[24] Doherty, W., Adler, N., Knox, A., Nolan, D., McGouran, J., Nikalje, A. P. G., Lokwani, D., Sarkate, A., Evans, P., Synthesis and Evaluation of 1,2,3-Triazole-Containing Vinyl and Allyl Sulfones as Anti-Trypanosomal Agents, *Eur. J. Org. Chem.*, **2017**, *1*, 175.

https://doi.org/10.1002/ejoc.201601221

[25] Shelke, R. N., Pansare, D. N., Khade, M. C., Jadhav, V. N., Pawar, C. D., Deshmukh, S.U., Sarkate, A. P., Gore N. S., Pawar, R. P., Shinde, D. B., Thopate, S. R., Synthesis of 2-((5-benzylidene-4-oxo- 4, 5-dihydrothiazol- 2-yl)-substituted amino acids as anticancer and antimicrobial agents, *Eur. Chem. Bull.*, **2019**, *8(2)*, 63. DOI: 10.17628/ecb.2019.8.63-70

[26] Kale, I. A., Gore, N. S., Sarkate, A. P., Sakhale, B. K., Khandare, A. L., Sinha, S. N., Karnik, K. S., Pansare, D. N., Peel extract associated oxidative green Dakin synthesis of some phenols, using aqueous banana extract catalyst, Eur. Chem. Bull., 2019, 8(5), 160. http://dx.doi.org/10.17628/ecb.2019.8.160-163.

Received: 16.07.2019.
Accepted: 11.03.2019.

AN INTERACTION MODE OF *N*-(DECYLOXYPHENYL)-*N*‘-(4-CHLOROBENZOYL)THIOUREA DOPANT IN CARBOXYMETHYL CELLULOSE (CMC) FOR SOLID POLYMER ELECTROLYTE

Wan M. Khairul,[a]* Saidatul Radhiah Ghazali,[b] M. I. N. Isa,[c] Adibah Izzati Daud[a,d] and Rafizah Rahamathullah[a,d]

Keywords: thiourea, carboxymethyl cellulose, conductive thin film

Alkoxy substituted arylthiourea derivatives provide excellent electronic properties due to the presence of rigid π-systems within their molecular framework. This study introduces a new thiourea derivative, *N*-(decyloxyphenyl)-*N*‘-(4-chlorobenzoyl)thiourea (**1A**), belongs to the compounds with general formula A-ArC(O)NHC(S)NHAr-D (A is an aryl group containing chloro (-Cl) substituent, in which acts as electron acceptor, while D represented as $–OC_nH_{2n+1}$, the alkoxy chain tail acts as electron donor). Due to its characteristic of D-π-A system, alkoxy thiourea derivatives are applied as a dopant in Carboxymethyl Cellulose (CMC) host material to form a conductive biopolymer solid polymer electrolyte (SPE) film. The formation of a biopolymer-thiourea complex (**1A-CMC**) has been analyzed through Fourier Transform Infrared (FTIR) spectroscopy and X-ray diffraction (XRD) to determine the interaction between CMC and thiourea derivative in the form of film as well as Electrical Impedance Spectroscopy (EIS) for their ionic conductivity behavior. The highest conductivity at ambient temperature (303K) exhibits 1.44 x 10^{-7} S cm^{-1} for CMC-thiourea complexation featuring chloro-substitution (**1A**). Indeed, biopolymer electrolyte materials featuring thiourea derivative as a dopant has great potential to be developed as an electrical conductor. Due to these findings, these so-called molecular wires candidate has opened wide possibilities to be applied in many microelectronic devices in the near future.

* Corresponding Authors
E-Mail: [a]wmkhairul@umt.edu.my
[a] [1]School of Fundamental Science, Universiti Malaysia Terengganu, 21030, Kuala Nerus, Terengganu, Malaysia
[b] Polymer Department, Faculty of Chemical Engineering Technology, TATI University College, 24000 Kemaman, Terengganu, Malaysia
[c] Frontier of Materials Research Group, Advanced Materials Team, Faculty of Science and Technology, Universiti Sains Islam Malaysia, Bandar Baru Nilai, 71800 Nilai, Negeri Sembilan, Malaysia
[d] [4]Faculty of Engineering Technology, Universiti Malaysia Perlis (UniMAP), Sungai Chuchuh, 02100 Padang Besar, Perlis, Malaysia

INTRODUCTION

Nowadays, thiourea derivatives have been used widely in numerous advanced materials application such as in drug development for pharmaceutical application,[1] chemical sensors for anions and gas detection,[2,3] active layer for photovoltaic solar cells and catalysis in promoting the cross-coupling reaction.[4,5]

The uniqueness of thiourea derivatives incorporating with varies functional group substitutions make them versatile compounds to be applied in advanced materials application. The presence of diprotic donor group insight thiourea derivatives plays a significant role in providing enough electron to the conjugated system of thiourea derivatives, in which, the π-conjugated system of thiourea derivatives make it as a promising candidate for molecular wires.

Currently, the development of molecular wires featuring conjugated polymers has become exceptional attention. There is an urgent need to explore the ideal materials in the form of the membrane to be applied in microelectronic devices. In this context, the synthesis and ability of thiourea derivatives bearing methyl substitution as a dopant in carboxymethyl cellulose (CMC) have been reported by our group in the previous occasion.[6] As a continuation of our previous work, a different type of withdrawing group involving chloro substitution of alkoxy thiourea was doped into CMC in demand to develop new biopolymer electrolyte film and further characterized the film using FTIR, XRD and AC-impedance spectroscopic studies. CMC is also well-known as a cellulose gum with the characteristic of anionic, soluble in water media, biodegradable and exhibit excellent mechanical properties.[7,8] However, the use of CMC itself as a polymer host gave a moderate conductivity performance. To overcome this issue, the use of suitable dopant into the polymer host system is needed to enhance the conductivity performance of solid polymer electrolytes.

In addition, the properties of dopant must be suited to the CMC properties in both chemical and mechanical aspects. Thiourea derivatives are known as versatile compounds consist of fair π-system with electronic conjugation on its structure that gave an enormous potential to be an ideal candidate as a dopant for CMC polymer host. Therefore, the purpose of this research was to prepare and characterize a novel thiourea-based conjugated compound prior to the formation of a solid conductive membrane to enhance the conductivity of CMC.

EXPERIMENTAL

Synthesis of *N*-decyloxyphenyl-*N*’-(chlorobenzoyl)thiourea(1A)

An equimolar amount of 4-chloro benzoyl chloride (5.50 g, 31.20 mmol), ammonium thiocyanate (2.40 g, 31.20 mmol) were suspended into 50 ml of acetone to afford an off-white solution. The solution was stirred at room temperature for ca. 4 hours followed by the addition of 4-decyloxy aniline (7.8 g, 31.20 mmol). The reaction was then put at reflux for another 1 hour until the observed color of the solution turned from off-white to white. After the reaction was adjudged completion by thin layer chromatography (hexane: dichloromethane: 2:3), the reaction mixture was cooled to room temperature and filtered. The off-white filtrate was added with ice cubes and filtered to yield a crude product of white precipitate. The white precipitate was then recrystallized from methanol to afford the white crystalline solid of the title compound, **1A** (3.40 g, 54 %).

Preparation of thiourea carboxymethyl cellulose (CMC) polymer electrolyte (1A-CMC)

The biodegradable film of solid polymer electrolyte (SPE) was prepared by the solution casting technique. 0.50 g CMC (obtained from standard supplier Across Organic Co.) was dissolved into 50 ml of water, while, in another different beaker, an equal amount of thiourea derivative **1A** was dissolved in 50 ml methanol with constant stirring at 30 – 40 °C. After that, the thiourea solution was added into CMC solution with continuous stirring to form homogenous dissolution. The mixture was then poured into a petri dish and allowed for slowly evaporation at ambient temperature for the formation of thin film (**1A-CMC**).

Electrical conductivity measurement of 1A-CMC

Electrical conductivity measurement was determined using HIOKI 3531 High-tester electrical impedance spectroscopy (EIS) in the frequency range 50 Hz – 1 MHz. The SPE sample of **1A-CMC** was cut into 2cm x 2cm (the same size as the stainless-steel blocking electrode and the sample was sandwiched between them.

RESULTS AND DISCUSSION

To prepare *N*-decyloxyphenyl-*N'*-(chlorobenzoyl) thiourea (**1A**), equimolar amounts of 4-chlorobenzoyl chloride and ammonium thiocyanate were reacted in acetone at room temperature for 4 h, then 4-decyloxy aniline was added and the reaction mixture was refluxed for 1 h. The synthetic pathway in the preparation of the final product of interest (**1A**) is as described in Scheme 1.

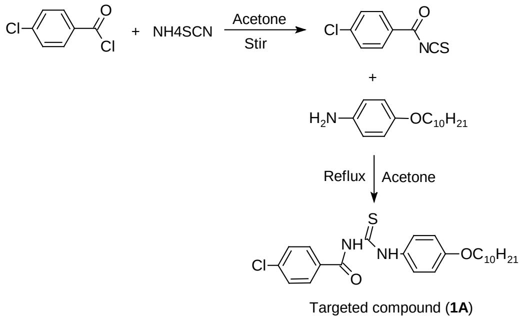

Scheme 1. Reaction pathway to the synthesis of **1A**.

The biodegradable film of solid polymer electrolyte (SPE) was prepared by the solution casting technique. An equal amount of thiourea derivative **1A** dissolved in methanol was mixed with an aq. solution of CMC and the mixture was left slowly to evaporate at ambient temperature for the formation of thin film (**1A-CMC**).

The bulk resistance (R_b) value was obtained from the plot of negative imaginary impedance versus the real part of impedance, in which the conductivity of the sample was calculated from Eq. 1:

$$\sigma = \frac{t}{R_b a} \qquad (1)$$

where

t is the thickness of the film,

a is for the film's area and

R_b represents bulk resistance of the film.

Characterisation of polymer electrolyte film (1A-CMC)

Fourier-Transform Infrared (FTIR) analysis was carried out to determine the occurrence of complexation between CMC and thiourea (**1A**) compound. CMC was adopted as a host polymer while **1A** acts as dopant material to enhance the conductivity performance of SPE film.

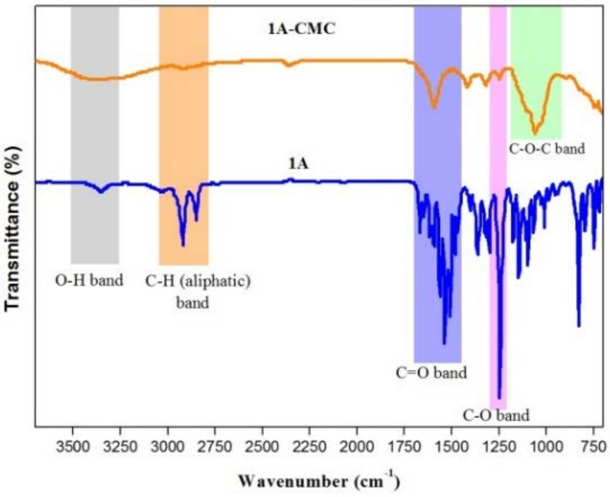

Figure 1. Overlay FTIR spectra of **1A-CMC** and its dopant (**1A**)

Fig.1 depicts the comparison of FTIR spectra to show evidence of the occurrence of complexation that has been taken place between CMC and **1A**.

From the above spectra, it was clearly shown that there are some changes in the wavenumber and intensity peaks of **1A** dopant upon the addition of CMC. The wavenumber and intensity of major absorption bands represent the main functional groups of **1A** decreases due to the existence of an interaction between **1A** with CMC and the interruption of amorphous nature of CMC to form new SPE film. In this sense, the presence of a new weak broad band of O-H group in the range of 3400-3200 cm^{-1} in the **1A-CMC** film indicates the functionality of –OH group of CMC and confirms the existence of polymer host in newly developed SPE film.

The strong C=O stretching band and C-O ether bands at 1650 cm^{-1} and 1176 cm^{-1} from **1A** is shifted within the range of 1700 – 1670 cm^{-1} and 1130-1140 cm^{-1} upon addition of CMC which represents asymmetric stretching carboxylate (COO$^-$) anions of (C=O) and (C-O) moieties functional group in the system.[9] Noticeable changes in wavenumber and intensity peak of these peaks prove that the interaction has occurred between **1A** as dopant and CMC host polymer to obtain the SPE film featuring **1A-CMC**. The existence of a strong peak at 1100 – 1000 cm^{-1} attributed to C-O-C stretching band in the SPE system also indicate the presence of polymer host in **1A-CMC**.

X-Ray diffraction study of 1A-CMC

XRD was used to reveal the nature of complexes of SPE film. The formation of complexes can be identified from the changes in diffraction peaks, the presence of new peak or/and absence of peak from the original position due to the increase of amorphousness of the sample. Fig.2 represents the overlaid XRD diffractogram of **1A** and **1A-CMC**.

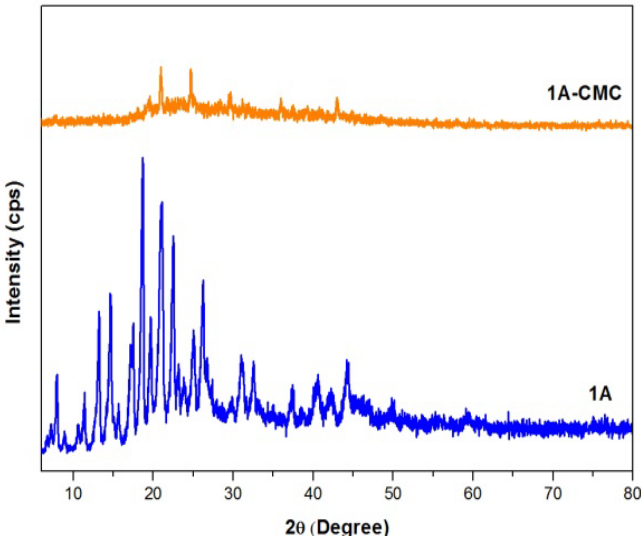

Figure 2. XRD diffractograms of CMC-thiourea SPE film (1A-CMC) and thiourea dopant (1A)

The XRD diffractogram of thiourea dopant (**1A**) at the ambient environment for 2θ from 6° to 60° shows many broad Bragg peaks at around ~15-25°, indicating semicrystalline nature. By adding CMC, the diffraction peaks become broader and less intense as shown for sample CMC-thiourea (**1A-CMC)** due to the increase of the amorphous content of thiourea which decreases the degree of crystallinity.[10] This, in turn, has increased the segmental mobility of the **1A-CMC** system and lowers the transition temperature T_g, which contributed to the increase in conductivity.

Conductivity study of 1A-CMC

The conductivity of **1A-CMC** was investigated from the EIS study conducted using HIOKI 3232-50 LCR Hi-tester interfaced with a computer in which the resultant Cole-Cole plot and conductivity graph of **1A-CMC** SPE film at elevated temperature reveal that the highest conductivity achieved is 1.44 x 10^{-7} S cm^{-1} at 303 K was obtained as in Fig. 3.

The high frequency of the obtained semicircle is related to the ionic conduction process in the bulk of the polymer electrolytes. While the semicircle possesses a low frequency attributed to the effect of electrode polarization in which related to the charge transfer process.[11] From the Cole-Cole plot, the information of the bulk resistant, R_b can be obtained to calculate the conductivity of the films. The bulk resistance, R_b can be retrieved from the intercept of the high-frequency semicircle and the low-frequency spike on the Z_r-axis. Equation 1 is used to calculate the conductivity, σ of **1A-CMC**.

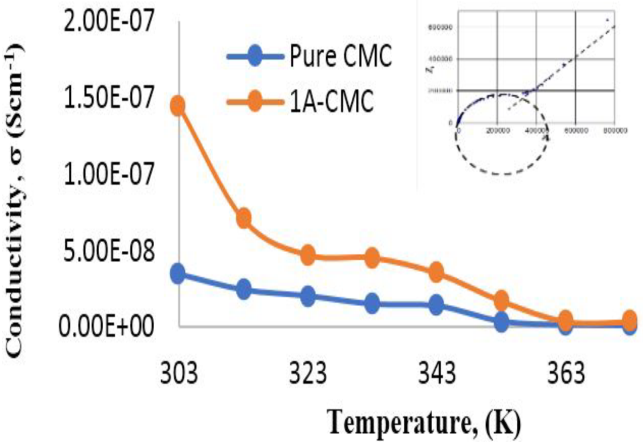

Figure 3. The values of conductivity of pure CMC and 1A-CMC (Inset: Cole-cole plot)

Predicted Molecular Structure of 1A-CMC complex

To predict the molecular structure of the complex between thiourea and CMC (**1A-CMC**), the Mulliken charges values are measured using theoretical calculation using TD-DFT B3LYP/6-31G (d, p) basis set. The Mulliken charges values on the selected atoms of thiourea dopant (**1A**) is listed in Table 1.

Table 1. Mulliken effective charges value of selected atom on thiourea dopant (**1A**)

Thiourea dopant	Mulliken charges			Thiourea-CMC complex	Calculated distance, Na$^+$ to O, Å	
	O (C=O Amide)	S	O (alkoxy)		O=C	–O$^-$
1A	-0.535	-0.262	-0.549	**1A-CMC**	2.2446	2.3108

From the Mulliken analysis, the charges on the oxygen atom of C=O amide are about two times higher than of sulfur atom of **1A**. While the values of charges observed for oxygen atoms of alkoxy were slightly similar to the oxygen atom of C=O amide. In this sense, we believed that the complexation is formed between the COO^-Na^+ of CMC and the oxygen of amide as a ‘head’ and another COO^-Na^+ of CMC to the oxygen alkoxy as a ‘tail’ due to the higher negative value of charges on oxygen atoms as depicted in Fig. 4. An attempt also has been made to optimize the complex formed between thiourea and CMC using the binding site of COO^-Na^+ to the oxygen carbonyl of amide and alkoxy oxygen which resulted in a significant interaction in which the distance between the two poles are in the range of 2.23 to 2.25 Å.

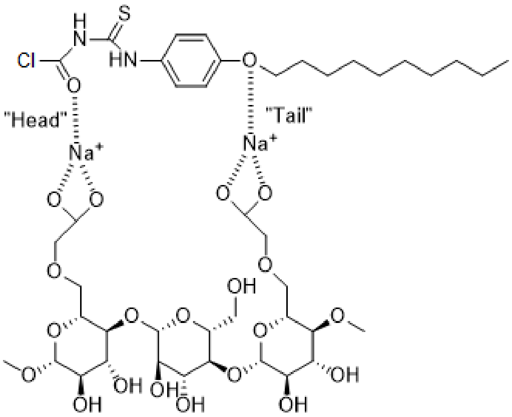

Figure 4. The proposed molecular structure of thiourea-CMC (**A1-CMC**) complex

CONCLUSION

Thiourea derivative featuring chloro substitution (**1A**) has been successfully synthesized and characterized using standard spectroscopic and analytical methods. In turn, **1A** has been doped into CMC host for the formation of SPE thin of **1A-CMC** *via* solution casting technique. The conductivity behavior of **1A-CMC** has been evaluated using electrical impedance spectroscopy (EIS). Results obtained revealed that, by addition of **1A** as a dopant in CMC host, the electrical conductivity of SPE film has increased from 10^{-9} to 10^{-7} Scm^{-1}. This study indicates that **1A** exhibits great promises and show excellent potential to be explored further as conductive biodegradable films for various electronic applications in the near future.

ACKNOWLEDGMENT

Special acknowledgment is dedicated to Ministry of Education (MOE), Malaysia for the funding of this research (FRGS 59253) and School of Fundamental Science Universiti Malaysia Terengganu (UMT) for research aid and facilities.

The paper was presented at Material Science Forum, Session 10: Biomaterials and Bioengineering in **AMSE-2019**, 21-24, July, Osaka, Japan.

REFERENCES

[1]Pingaew, R., Prachayasittikul, V., Anuwongcharoen, N., Prachayasittikul, S., Ruchirawat, S. and Prachayasittikul, V., Synthesis and molecular docking of N,N′-disubstituted thiourea derivatives as novel aromatase inhibitors. *Bioorg. Chem.*, **2018**, *79*, 171-178.

https://doi.org/10.1016/j.bioorg.2018.05.002

[2]Khairul, W. M., Hasan, M. A., Daud, A. I., Zuki, H. M., Kubulat, K., Kadir, M. A., Theoretical and experimental investigation of pyridylthiourea derivatives as ionophores for Cu(II) ion detection, *Malays. J. Anal. Sci.*, **2016**, *20*, 73-84. https://doi.org/10.17576/mjas-2016-2001-08

[3]Daud, A. I., Khairul, W. M., Mohamed H., Zuki, K., Kubulat, K., Synthesis and characterization of N-(4-Aminophenylethynylbenzonitrile)-N′-(1-naphthoyl) thiourea as a single molecular chemosensor for carbon monoxide sensing, *J. Sulfur. Chem.*, **2014**, *35(6),* 691-699. https://doi.org/10.1080/17415993.2014.954248

[4]Karthika, P., Ganesan, S., Thomas, A., Rani, T. M. S., Prakash, M., Influence of synthesized thiourea derivatives as a prolific additive with tris (1, 10-phenanthroline) cobalt(II/III) bis/tris (hexafluorophosphate)/hydroxypropyl cellulose gel polymer electrolytes on dye-sensitized solar cells, *Electrochim. Acta*, **2019**, *298*, 237-247.

https://doi.org/10.1016/j.electacta.2018.12.099

[5]Rahamathullah, R., Khairul, W. M., Kubulat, K., Hussin, Z. M., Influence of curcumin as a natural photosensitizer in the conductive thin film of alkoxy cinnamoyl substituted thiourea. *Main Group Chem.*, **2015**, *14(3),* 185-198. https://doi.org/10.3233/MGC-150162

[6]Ghazali, S. R., Kubulat, K. M.. Isa, I. N., Samsudin, A. S., Khairul, W. M., Contribution of methyl substituent on the conductivity properties and behavior of CMC-alkoxy thiourea polymer electrolyte. *Mol. Cryst. Liq. Cryst*., **2014**, *604(1)*, 126-141. https://doi.org/10.1080/15421406.2014.968058

[7]Balaya, P., Goyal, P. S., Non-Debye conductivity relaxation in a mixed glassformer system, *J. Non-Cryst. Solids*, **2005**, *351(19-20),* 1573-1576.

https://doi.org/10.1016/j.jnoncrysol.2005.03.045

[8]Marcì, G., Mele, G., Palmisano, L., Pulito, P., Sannino, A., Environmentally sustainable production of cellulose-based superabsorbent hydrogels, *Green Chemistry*, **2006**, *8(5),* 439-444. https://doi.org/10.1039/b515247j

[9]Pushpamalar, V. Langford, S. J. Ahmad, M. Lim, Y. Y. Optimization of reaction conditions for preparing carboxymethyl cellulose from sago waste. *Carbohyd. Polym.*, **2006**, *64(2),* 312-318. https://doi.org/10.1016/j.carbpol.2005.12.003

[10]Yang, S., Fu, S., Liu, H., Zhou, Y., Li, X., Hydrogel beads based on carboxymethyl cellulose for removal heavy metal ions. *J. Appl. Polym. Sci.*, **2011**, *119(2),* 1204-1210. https://doi.org/10.1002/app.32822

[11]Ho, C. H., Shieh, C. Y., Tseng, C. L., Chen, Y. K., Lin, J. L., Decomposition pathways of glycolic acid on titanium dioxide. *J. Catal.*, **2009**, *261(2),* 150-157. https://doi.org/10.1016/j.jcat.2008.11.008

Received: 07.04.2019.
Accepted: 31.05.2019.

DETERMINATION OF ANTIOXIDANT AND ACIDITY REGULATORS AS ADDITIVES IN DIFFERENT FRUIT JUICES OF INDIA

Shazia Khanum Mirza[a]* and Sayyad Sultan Kasim[a]

Keywords: Fruit juices; acidity regulators; citric acid; antioxidants; ascorbic acid.

The increasing demand for ready-to-drink juices has led to challenges for food distributors regarding the safety and quality of their foods hence food additives are added to foods to keep them fresh, control its pH and improve the flavor, texture, color or taste and appearance. The present work aimed at the quantitative determination of additives as ascorbic acid and citric acid in a variety of fruit juices of India using the classical titration method, to check whether the current uses of these additives are according to the Food Safety and Standard Authority of India (FSSAI). Consuming too much amount of vitamin C may increase the amount of oxalate in your kidneys, which has the potential to lead to kidney stone problem. The high intake of citric acid leads to stomach pain, diarrhea, nausea or vomiting, increased sweating and fast heart rate. In this study, we have selected 14 different popular juice samples which are consumed most by Indian children. Each sample was analyzed for organoleptic or physical tests such as color, texture, flavor, taste and pH. These findings indicated that the current use of ascorbic acid and citric acid in all juices by the fruit juice industry is below the permitted limit of FSSAI and are safe for the consumption by Indian children.

* Corresponding Authors
E-Mail: mirzabaig1184@gmail.com
[a] Department of Chemistry, Maulana Azad College of Arts, Science and Commerce, Aurangabad- 431001, (M.S), India.

Introduction

Nowadays most people tend to eat the ready-made food available in the market rather than preparing it at home. Such foods contain some additives and preservatives so that their quality and flavor are maintained and bacteria and yeasts do not spoil them. Current trends show that increasing technology and inclusion of packaged foods in the diets of modern society leads to an increase in the use and need of food additives.

The USFDA defines food additives as "any substance, the intended use of which results or may reasonably be expected to result directly or indirectly if it is becoming a component or otherwise affecting the characteristics of any food".[1]

Direct additives are those that are added intentionally to food for a specific purpose, while indirect additives are those to which the food is exposed during processing, packaging or storing.[2] Food additives are substances which are added to food which improve the flavor, texture, color, taste, appearance, function as processing aid or are chemical preservatives. Food additives as non-nutritive substances added intentionally to food, generally in small quantities to improve its appearance, flavor, texture or storage property.[3,4]

Food safety is a global problem and a large number of consumers worldwide face a variety of food safety risks each year. The majority of food safety incidents are caused by illegal activities, especially by abuse of food additives and even illegal use of chemical additives. The synthetic food additives react to the cellular component of the body leading to the various physiological effects. Many effects like food allergies, food intolerance, cancer, attention deficit hyperactivity disorder (ADHD), brain damage, nausea, cardiac disease among others have been reported.[5] Additive has been used for many years to preserve, flavor, blend, thicken and color foods and have played an important and essential role in reducing serious nutritional deficiencies.[6] There are thousands of food additives found in food. USFDA maintains a list of over 3000 ingredients in its food additive database.[7] Additives may cause different allergies, asthma, high fever, and certain reactions such as rashes, vomiting, headache, and tight chest.[6] The use of food additives in food manufacturing has been a public health issue for many years.[8]

The increasing demand for ready-to-drink juices has led to challenges for food distributors regarding the safety and quality of their foods. Acidity regulators are used to changing or otherwise control alkalinity and acidity of foods. Acidity regulators or pH control agents are the food additives added to improve or maintain the pH of the food. They can be organic acids or mineral acids, bases, neutralizing agents or buffering agents. Acidity regulators are used to altering and controlling the acidity or alkalinity at a specific level important for processing, taste and food safety.

Citric acid is a weak organic acid. It is a white crystalline powder extracted from citrus fruits. It has a distinct sour taste. The molecular weight of citric acid is 192.09. The molecular formula is $C_6H_8O_7$. The E number of citric acid is E330. The citric acid has many uses, including food preservatives. It has a pleasant citrus flavor that works well in beverages and juices and crunchy snacks. Citric acid is used both as a natural flavor enhancer and preservative in a variety of foods such as jams, jellies, canned fruits and vegetables, ice creams, fruit drinks, candies and carbonated drinks and beverages. It helps to regulate acidity, is an antioxidant and maintains the pH of the food. Many canned food contains added citric acid because it helps to extend the shelf life of the product as well as enhance the flavor.

DOI: http://dx.doi.org/10.17628/ecb.2019.8.235-238

The most common adverse symptom of high intake of citric acid includes stomach pain, diarrhea, nausea or vomiting, loss of appetite, and increased sweating, fast heart rate, restless feeling, and slow breathing. The uncommon symptoms are cloudy urine, fever, headache and increase in blood pressure. Sometimes pain in muscles also occurs.

The oxidation process spoils most food, especially those with high-fat contents. Antioxidants are the food additives which increase the shelf life of foods by inhibiting oxidation. Some of the antioxidants foods additives combine with oxygen to prevent oxidation and others prevent the oxygen from reacting with the food leading to its spoilage. In the absence of antioxidant food additives, oxidation of unsaturated fats takes place, rendering a foul smell and discoloration of food. Oxidation is a chemical reaction that can produce free radicals leading to chain reactions that may damage cells. Antioxidant terminates these chain reactions. Fats turn rancid when exposed to oxygen.

Ascorbic acid is also commonly known as Vitamin C. Its E number is 300. It acts as an antioxidant. It is used in many foods as an anti-oxidizing agent. The molecular weight of vitamin C is 176.12. The chemical formula of vitamin C is $C_6H_8O_6$.

There are many juices and fruit drinks available in the market which contains added Vitamin C. There are many benefits of using antioxidant food additives. If we read the ingredient list for fruit juices and drinks, cereals, fruit-flavored candies, cured meats, cereals and frozen fruits, ascorbic acid is added. An antioxidant is a molecule that inhibits the oxidation of other molecules. Antioxidants prevent or inhibit the oxidation process. The most common antioxidant additives are ascorbic acid i.e., vitamin C.

The most common side effect of high vitamin C intake is digestive distress and kidney stones. If it is taken in very high doses, it exhibits common side effects including headache, feeling faint, redness and warm feeling of the skin or flushing, nausea, vomiting or diarrhea, heartburn, and abdominal cramps. The most common side effect of high vitamin C intake is digestive distress and kidney stones. Consuming too much amount of vitamin C may increase the amount of oxalate in your kidneys, which may lead to kidney stone problem. The recommended daily intake of vitamin C is 90 mg for men and 75 mg for women.[9]

Experimental

General

The chemicals used for analysis were of A.R. Grade and were from S.D. fine chemicals. They were used without further purification. All the experimental vessels and storage containers were Pyrex glass.

In this research work, each sample was analyzed for organoleptic or physical tests such as color, texture, flavor, taste and pH measurement.

Qualitative analyses of different juice were done for additives content such as acidity regulator as citric acid and antioxidant as ascorbic acid. The 14 different packaged fruit juices were selected, which are most popular among the children of India, from the local market of Aurangabad, India. They were then frozen in plastic bags in household freezer (-20 °C) and kept until analysis. The packaged fruit juice samples, as shown in Table 1, were selected. All these juices are made in India.

Table 1. Packaged fruit juice samples selected for analysis from the Indian market

Code	Indian Brand Name	Type of Fruit Juice
A	Appy	Apple juice
B	Frooti	Mango juice
C	Real fruit power	Mix fruit juice
D	Tropicana Mixed Fruit	Mix fruit juice
E	B-Natural Orange	orange juice
F	Minute Made Apple	Apple juice
G	Maaza Refresh	Mango juice
H	Alo Fruit Berries	Berry juice
I	Enerzol Orange	Orange drink
J	Tropicana Pineapple	pineapple juice
K	Paper Boat Alphaso Aam	Mango juice
L	Delmonte Pineapple	Pineapple Juice
M	Pride Pinch Lemon	Carbonate Lemon
N	Fruit Valley Mix	Mix fruit juice

Determination of pH

Exactly 25 mL of liquid sample was weighed and transferred to a 100 mL dry beaker. It was dissolved in a small amount of boiled and cooled distilled water by little warming. The volume was made to 100 mL by using decarbonized distilled water. The pH of this solution was recorded on a pH meter at room temperature.

Determination of acidity regulator as citric acid (E330)

Accurately weighed about 2 g sample was mixed in 50 mL decarbonized distilled water, warmed for about 15-20 min and cooled to room temperature. In the case of dilute samples, 10 mL of sample solution was mixed with is 20 mL of distilled water. The solution was titrated against 0.1 N sodium hydroxide solution using phenolphthalein solution as an indicator.

Determination of acidity regulator as acetic acid (E260)

About 10 mL of the sample was taken in a conical flask and 20 mL of distilled water was added in it. It was boiled for about 5 min, cooled to room temperature and was titrated against the 0.1 N NaOH solution using phenolphthalein as an indicator.

Determination of antioxidant as ascorbic acid (E330)

Accurately about 10 mL of the sample was taken in a conical flask and 25 mL of dilute H_2SO_4 was added in it. This solution is titrated with the 0.1 N iodine solution using starch as an indicator.

Results

The experimental results of the determination of additives in the selected fruit juices are depicted in the Tables 2-4.

Table 2. Physical/organoleptic tests of packaged fruit juices

Code	Colour	Flavor	Taste
A	Light brown	Apple	Sweet
B	Light yellow	Mango	Sweet
C	Light red	Mix fruit	Sweet
D	Light orange	Mix fruit	Sweet
E	Light orange	Orange	Sweet and sour
F	Light brown	Apple	Sweet
G	Dark yellow	Mango	Sweet
H	Light violet	Berry	Sweet and sour
I	Orange	Orange	Sweet and sour
J	Light yellow	Pineapple	Sour
K	Dark yellow	Mango	Sweet
L	Light yellow	Pineapple	Sweet
M	Colorless	Lemon	Sour
N	Light brown	Mix fruit	Sweet

Table 3. Determination of pH and ascorbic acid as an antioxidant in packaged fruit juices

Code	pH	Ascorbic acid %	Code	pH	Ascorbic acid %
A	5.60	1.58	H	6.2	3.34
B	3.64	1.32	I	3.30	2.46
C	5.16	2.46	J	3.80	2.90
D	5.47	2.81	K	5.90	1.84
E	3.60	3.34	L	4.25	2.70
F	5.50	1.58	M	2.35	1.58
G	5.80	1.60	N	4.19	2.46

Table 4. Determination of citric acid as an acidity regulator in packaged fruit juices.

Code	Citric acid, %	Code	Citric acid, %
A	3.26	H	3.07
B	3.64	I	2.49
C	2.68	J	4.73
D	4.41	K	2.75
E	5.21	L	3.71
F	3.52	M	4.80
G	2.49	N	2.43

Discussion

All the Juice samples were selected for the qualitative analysis of additives present in it. Each juice samples was analyzed for pH, antioxidant as ascorbic acid and acidity regulator as citric acid. The pH of juices changes along a wide scale, the highest pH, 6.20 is of Alo berries juice and the lowest pH, 2.35, is of pride pinch lemon. The values for each sample can be seen in Table 3.

The most significant amount of ascorbic acid, 3.34 %, was found in B Natural orange juice and Alo fruit Berries, the lowest ascorbic acid was detected in Frooti juice 1.32 %, Minute Made apple juice 1.58%, pride pinch 1.58 % and Maaza juice 1.60 %. Real fruit power, Enerzol orange and Fruit valley juice contain 2.46% of ascorbic acid. Delmonte fruit juice, Tropicana mix juice and Tropicana pineapple juice contain 2.70 %, 2.81 %, 2.90 % respectively as shown in Table 3.

The maximum amount of citric acid present in the B natural orange juice 5.21 %. The minimum contents of citric acid are in fruity valley mix juice 2.43 % and Paperboat juice alphanso 2.75 %. The other values can be seen in (Table 4).

Al-Harthy and Abukhader[10] identified food additives content in selected snack foods and beverages sold in the Omani market. Citric acid is the most common one and frequently used in all the products. Brima and Abbas[11] analyzed the drinks from the local market of the Kingdom of Saudi Arabia. They reported that the citric acid is used as an additive in different drinks to improve flavor and taste. His results also showed a range of concentration in different samples. 22 % of the samples were shown to have citric acid concentration is higher than 3 g L^{-1}. They suggested that this data can be used to formulate public health awareness.

Conclusion

In this study, we have taken 14 different popular juice samples, consumed most by the Indian children, which are available in the supermarkets of Aurangabad, India. The objective of this research was to evaluate the physical and chemical parameters. Each sample was analyzed for organoleptic or physical tests such as color, texture, flavor, taste and the pH measurement. These findings indicated that the current use of ascorbic acid and citric acid in juices by the fruit juice industry is in below upper limit of FSSAI and are safe for the consumption of children of India.

Acknowledgments

Thanks are due to the University Grants Commission, India for the Senior Research Fellowship to SKM.

We thank Ms. Fateema Rafiq Zakaria, Chairperson of Dr. Rafiq Zakaria Campus, Maulana Azad College of Arts, Science and Commerce, Aurangabad, India, for her constant encouragement and providing laboratory facilities for this research work.

References

[1]Jacob, M. B., *The Chemical Analysis of Food & Food Products*, CBS Publishers, 3rd Edition, **1999**, 540 and 725-730.

[2]Kirk, R. S., Person, R. S., *Composition and Analysis of Foods*, Addison Wesley Harlow, 9th Edition, **1991**, 263-265.

[3]Chatwal, G. R., *Analytical Chemistry*, Himalaya Publishing House, New Delhi, 1st Edition, **2008**, 75-86.

[4]Kaur, H., *Analytical Chemistry*, Himalaya Publishing House, New Delhi, 3rd Edition, **2015**, 81-87.

[5]Sachithananthan V., A study on the consumer awareness of food additives in packaged food and their effects on health in Abha region, Saudi Arabia, *J. Food Process. Preserv*., **2017**, *1*, 14-27.

[6]Mumeen, H. A. A., Risikat, A. N., Sururah, A., Food its Preservatives, Additives and Applications, *Int. J. Chem. Biochem. Sci*., **2012**, *1*, 36-47.

[7]Kaptan, B., Kayisoglu, S., Consumer's attitude towards food additives, *J. Food Nutr. Res*., **2015**, *2*, 21-25.

[8]Saltmarsh M., *Essential Guide to Food Additives*, The Royal Society of Chemistry, Cambridge, U.K, 4th Edition, **2013**.

[9]The Office of Dietary Supplements (ODS) of the National Institutes of Health (NIH), Vitamin C, https://ods.od.nih.gov/factsheets/VitaminC-Consumer/

[10]Al-Harthy, A. M., Abukhader, M. M., Food Additives Content in Selected Snack Foods & Beverages and Public Perception of E-Numbers in Muscut, Oman, *Athens J. Health*, **2017**, *4*, 83-95. https://doi.org/10.30958/ajh.4-1-5

[11]Brima, E. I., Abbas, A. M., Determination of citric acid in soft drinks, juice drinks and energy drinks using titration, *Int. J. Chem. Stud*., **2014**, *1*, 30-34.

This research paper was presented at the "International Symposium on Exploring New Horizons in Chemical Sciences," 10th-12th January 2019, Aurangabad, India

Received: 30.03.2019.

Accepted: 28.07.2019.